
RANDOM GENETIC DRIFT SETS AN UPPER LIMIT ON mRNA SPLICING ACCURACY IN METAZOANS

Florian Bénétière, Anamaria Necșulea, Laurent Duret

Laboratoire de Biométrie et Biologie Évolutive, [Université Lyon 1](#), [UMR CNRS 5558](#), Villeurbanne, France.

Correspondence: Laurent.Duret@univ-lyon1.fr

June 6, 2023

Abstract

1 Most eukaryotic genes undergo alternative splicing (AS), but the overall functional significance
2 of this process remains a controversial issue. It has been noticed that the complexity of
3 organisms ([assayed by the number of distinct cell types](#)) correlates positively with their
4 genome-wide AS rate. This has been interpreted as evidence that AS plays an important
5 role in adaptive evolution by increasing the functional repertoires of genomes. However, this
6 observation also fits with a totally opposite interpretation: given that ‘complex’ organisms
7 tend to have small effective population sizes (N_e), they are expected to be more affected by
8 genetic drift, and hence more prone to accumulate deleterious mutations that decrease splicing
9 accuracy. Thus, according to this “drift barrier” theory, the elevated AS rate in complex
10 organisms might simply result from a higher splicing error rate. To test this hypothesis, we
11 [analyzed](#) 3,496 transcriptome sequencing samples to quantify AS in 53 metazoan species
12 spanning a wide range of N_e values. Our results show a negative correlation between N_e
13 proxies and the genome-wide AS rates among species, consistent with the drift barrier
14 hypothesis. This pattern is dominated by low abundance isoforms, which represent the vast
15 majority of the splice variant repertoire. We show that these low abundance isoforms are
16 depleted in functional AS events, and most likely correspond to errors. Conversely, the AS
17 rate of abundant isoforms, which are relatively enriched in functional AS events, tends to be
18 lower in more complex species. All these observations are consistent with the hypothesis
19 that variation in AS rates across metazoans reflects the limits set by drift on the capacity of
20 selection to prevent gene expression errors.

21 **Keywords** Alternative splicing · Random genetic drift · Life history traits · Effective
22 population size · dN/dS · Splice variants · Non-adaptive models · N_e

23 **Introduction**

24 Eukaryotic protein-coding genes are interrupted by introns, which have to be excised from the primary
 25 transcript to produce functional mRNAs that can be translated into proteins. The removal of introns from
 26 primary transcripts can lead to the production of diverse mRNAs, *via* the differential use of splice sites. This
 27 process of alternative splicing (AS) is widespread in eukaryotes (Chen *et al.*, 2014), but its ‘raison d’être’
 28 (adaptive or not) remains elusive. Numerous studies have shown that some AS events are functional, *i.e.*
 29 that they play a beneficial role for the fitness of organisms, either by allowing the production of distinct
 30 protein isoforms (Graveley, 2001) or by regulating gene expression post-transcriptionally (McGlinicy and
 31 Smith, 2008; Hamid and Makeyev, 2014). However, other AS events are undoubtedly not functional. Like any
 32 biological machinery, the spliceosome occasionally makes errors, leading to the production of aberrant mRNAs,
 33 which represent a waste of resources and are therefore deleterious for the fitness of the organisms (Hsu and
 34 Hertel, 2009; Gout *et al.*, 2013). The splicing error rate at a given intron is expected to depend both on the
 35 efficiency of the spliceosome and on the intrinsic quality of its splice signals. **The information required in cis**
 36 **for the removal of each intron resides in 20 to 40 nucleotide sites**, located within the intron or its flanking
 37 exons (Lynch, 2006). **Besides the two splice sites that are essential for the splicing reaction (almost always**
 38 **GT for the donor and AG for the acceptor), all other signals tolerate some sequence flexibility.** Population
 39 genetics principles state that the ability of selection to promote beneficial mutations or eliminate deleterious
 40 mutations depends on the intensity of selection (s) relative to the power of random genetic drift (defined by
 41 the effective population size, N_e): if the selection coefficient is sufficiently weak relative to drift ($|N_e s| < 1$),
 42 alleles behave as if they are effectively neutral. Thus, random drift sets an upper limit on the capacity
 43 of selection to prevent the fixation of alleles that are sub-optimal (Kimura *et al.*, 1963; Ohta, 1973). This
 44 so-called “drift barrier” (Lynch, 2007) is expected to affect the efficiency of all cellular processes, including
 45 splicing. Hence, species with low N_e should be more prone to make splicing errors than species with high N_e .
 46 The extent to which AS events correspond to functional isoforms or to errors is a contentious is-
 47 sue (Bhuiyan *et al.*, 2018; Tress *et al.*, 2017b; Blencowe, 2017; Tress *et al.*, 2017a). In humans,
 48 **the set of transcripts produced by a given gene generally consists of one major transcript (the ‘ma-**
 49 **major isoform’), which encodes a functional protein, and of multiple minor isoforms (splice variants),**
 50 **present in relatively low abundance, and whose coding sequence is frequently interrupted by prema-**
 51 **ture termination codons (PTCs) (Tress *et al.*, 2017a; González-Porta *et al.*, 2013). Ultimately, less than**
 52 **1% of human splice variants lead to the production of a detectable amount of protein (Abascal *et al.*,**
 53 **2015). Furthermore, comparison with closely related species showed that AS patterns evolve very**
 54 **rapidly (Barbosa-Morais *et al.*, 2012; Merkin *et al.*, 2012) and that alternative splice sites present little evi-**
 55 **dence of selective constraints (Pickrell *et al.*, 2010). All these observations are consistent with the hypothesis**
 56 **that a vast majority of splice variants observed in human transcriptomes simply correspond to erroneous**
 57 **transcripts (Pickrell *et al.*, 2010). However, some authors argue that a large fraction of AS events might in fact**
 58 **contribute to regulating gene expression. Indeed, PTC-containing splice variants are recognized and degraded**
 59 **by the non-sense mediated decay (NMD) machinery. Thus, AS can be coupled with NMD to modulate gene**
 60 **expression at the post-transcriptional level (McGlinicy and Smith, 2008; Hamid and Makeyev, 2014). This**

61 **AN-NMD regulatory process** does not involve the production of proteins and does not necessarily imply
 62 strong evolutionary constraints on splice sites. Thus, based on these observations, it is difficult to firmly
 63 refute selectionist or non-adaptive models.

64 The analysis of transcriptomes from various eukaryotic species showed substantial variation in AS rates
 65 across lineages, with the highest rate in primates (Barbosa-Morais *et al.*, 2012; Chen *et al.*, 2014; Mazin
 66 *et al.*, 2021). Interestingly, the genome-wide average AS level was found to correlate positively with the
 67 complexity of organisms (approximated by the number of cell types) (Chen *et al.*, 2014). This correlation
 68 was considered as evidence that AS contributed to the evolution of complex organisms by increasing the
 69 functional repertoire of their genomes (Chen *et al.*, 2014). This pattern is often presented as an argument
 70 supporting the importance of AS in adaptation (Verta and Jacobs, 2022; Singh and Ahi, 2022; Wright *et al.*,
 71 2022). However, this correlation is also compatible with a totally opposite hypothesis. Indeed, eukaryotic
 72 species with the highest level of complexity correspond to multi-cellular organisms with relatively large body
 73 size, which tend to have small effective population sizes (N_e) (Lynch and Conery, 2003; Figuet *et al.*, 2016).
 74 Thus, the higher AS rate observed in ‘complex’ organisms might simply reflect an increased rate of splicing
 75 errors, resulting from the effect of the drift barrier on the quality of splice signals (Bush *et al.*, 2017).

76 To assess this hypothesis and evaluate the impact of genetic drift on alternative splicing patterns, we quantified
 77 AS rates in 53 metazoan species, covering a wide range of N_e values, and for which high-depth transcriptome
 78 sequencing data were available. We show that the genome-wide average AS rate correlates negatively with
 79 N_e , in agreement with the drift barrier hypothesis. This pattern is mainly driven by low abundance isoforms,
 80 which represent the vast majority of splice variants and most likely correspond to errors. Conversely, the
 81 AS rate of abundant splice variants, which are enriched in functional AS events, show the opposite trend.
 82 These results support the hypothesis that the drift barrier sets an upper limit on the capacity of selection to
 83 minimize splicing errors.

84 Results

85 Genomic and transcriptomic data collection

86 To analyze variation in AS rates across metazoans, we examined a collection of 69 species for which
 87 transcriptome sequencing (RNA-seq) data, genome assemblies, and gene annotations were available in public
 88 databases. We focused on vertebrates and insects, the two metazoan clades that were the best represented in
 89 public databases when we initiated this project. To be able to compare average AS rates across species, we
 90 needed to control for several possible sources of biases. First, given that AS rates vary across genes (Saudemont
 91 *et al.*, 2017), we had to analyze a common set of orthologous genes. For this purpose, we extracted from
 92 the BUSCO database (Seppey *et al.*, 2019) a reference set of single-copy orthologous genes shared across
 93 metazoans (N=978 genes), and searched for their homologues in each species in our dataset. We retained for
 94 further analyses those species for which at least 80% of the BUSCO metazoan gene set could be identified
 95 (N=67 species; see Materials & Methods). Second, we had to ensure that RNA-seq read coverage was
 96 sufficiently high in each species to detect splicing variants. Indeed, to be able to detect AS at a given intron, it
 97 is necessary to analyze a minimal number of sequencing reads encompassing this intron (we used a threshold

of $N=10$ reads). To assess the impact of sequencing depth on AS detection, we conducted a pilot analysis with two species (*Homo sapiens* and *Drosophila melanogaster*) for which hundreds of RNA-seq samples are available. **This analysis (detailed in Supplementary Fig. 1) revealed that AS rate estimates are very noisy when sequencing depth is limited, but that they converge when sequencing is high enough.** We therefore kept for further analysis those species for which the median read coverage across exonic regions of BUSCO genes was above 200 (Supplementary Fig. 1). Our final dataset thus consisted of 53 species (15 vertebrates and 38 insects; Fig. 1A), and of 3,496 RNA-seq samples (66 *per* species on average). In these species, the **number of analyzable annotated introns (i.e. encompassed by at least 10 reads)** among BUSCO genes ranges from 2,032 to 10,981 (which represents 88.6% to 99.6% of their annotated introns; Supplementary Tab. 1). **It should be noted that analyzed samples originate from diverse sources; however, they are very homogenous in terms of sequencing technology (99% of RNA-seq samples sequenced with Illumina platforms; refer to Data10-supp.tab in the Zenodo data repository).**

110 Proxies for the effective population size (N_e)

Effective population sizes (N_e) can in principle be inferred from levels of genetic polymorphism. However, population genetics data are lacking for most of the species in our dataset. We therefore used two life history traits that were previously proposed as proxies of N_e in metazoans (Waples, 2016; Weyna and Romiguier, 2020; Figuet *et al.*, 2016): body length and longevity (Materials & Methods; Supplementary Tab. 2). An additional proxy for N_e can be obtained by studying the intensity of purifying selection acting on protein sequences, through the dN/dS ratio (Kryazhimskiy and Plotkin, 2008). To evaluate this ratio, we aligned 922 BUSCO genes, reconstructed the phylogenetic tree of the 53 species (Fig. 1A) and computed the dN/dS ratio along each terminal branch (Materials & Methods).

We note that these three proxies provide "inverse" estimates of N_e , meaning that species with high longevity, large body length and/or elevated dN/dS values tend to have low N_e values. As expected, these different proxies of N_e are positively correlated with each other ($p < 1 \times 10^{-3}$, Fig. 1B,C). We note however that these correlations are not very strong. **It thus seems likely that none of these proxies provides a perfect estimate of N_e .** To take phylogenetic inertia into account, all cross-species correlations presented here were computed using Phylogenetic Generalized Least Squared (PGLS) regression (Freckleton *et al.*, 2002).

125 Alternative splicing rates are negatively correlated with N_e proxies

To quantify AS rates, we mapped RNA-seq data of each species on the corresponding reference genome assembly. We detected sequencing reads indicative of a splicing event (hereafter termed 'spliced reads'), and inferred the corresponding intron boundaries. We were thus able to validate the coordinates of annotated introns and to detect new introns, not present in the annotations. For each intron detected in RNA-seq data, we counted the number of spliced reads matching with its two boundaries (N_s) or sharing only one of its boundaries (N_a), as well as the number of unspliced reads covering its boundaries (N_u) (Fig. 2A). We then computed the relative abundance of this spliced isoform compared to other transcripts with alternative splice boundaries ($RAS = \frac{N_s}{N_s + N_a}$) or compared to unspliced transcripts ($RANS = \frac{N_s}{N_s + \frac{N_u}{2}}$).

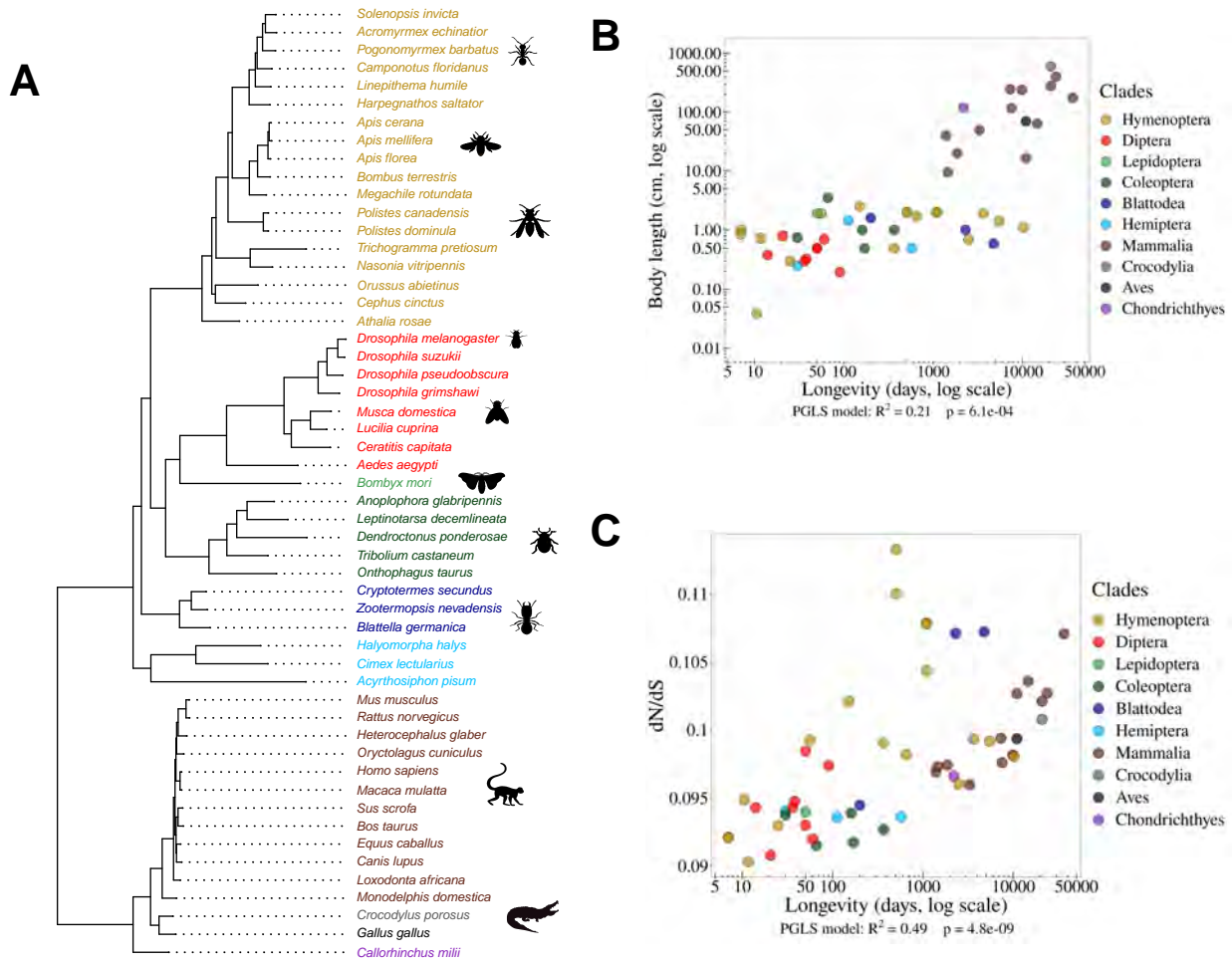


Figure 1: **Species phylogeny and N_e proxies.** **A:** Phylogenetic tree of the 53 studied species (15 vertebrates and 38 insects). **B:** Relationship between body length (cm, log scale) and longevity (days, log scale) of the organism. Each dot represents one species (colored by clade, as in the species tree in panel A). **C:** Relationship between longevity (days, log scale) and the dN/dS ratio on terminal branches of the phylogenetic tree (Materials & Methods). **B,C:** PGLS stands for Phylogenetic Generalized Least Squared regression, which takes into account phylogenetic inertia (Materials & Methods).

134

135 To limit measurement noise, we only considered introns for which both RAS and RANS could be computed
 136 based on at least 10 reads (Materials & Methods). In all species, both RAS and RANS metrics show clearly
 137 bimodal distributions (Fig. 2B,C): the first peak (mode < 5%) corresponds to ‘minor introns’, whose splicing
 138 occurs only in a minority of transcripts of a given gene, whereas the second one (mode > 95%) corresponds
 139 to the introns of major isoforms. It has been previously shown that in humans, for most genes, one single
 140 transcript largely dominates over other isoforms (Tress *et al.*, 2017a; Gonzàlez-Porta *et al.*, 2013). Our
 141 observations indicate that this pattern is generalized across metazoans. For the rest of our analyses, we

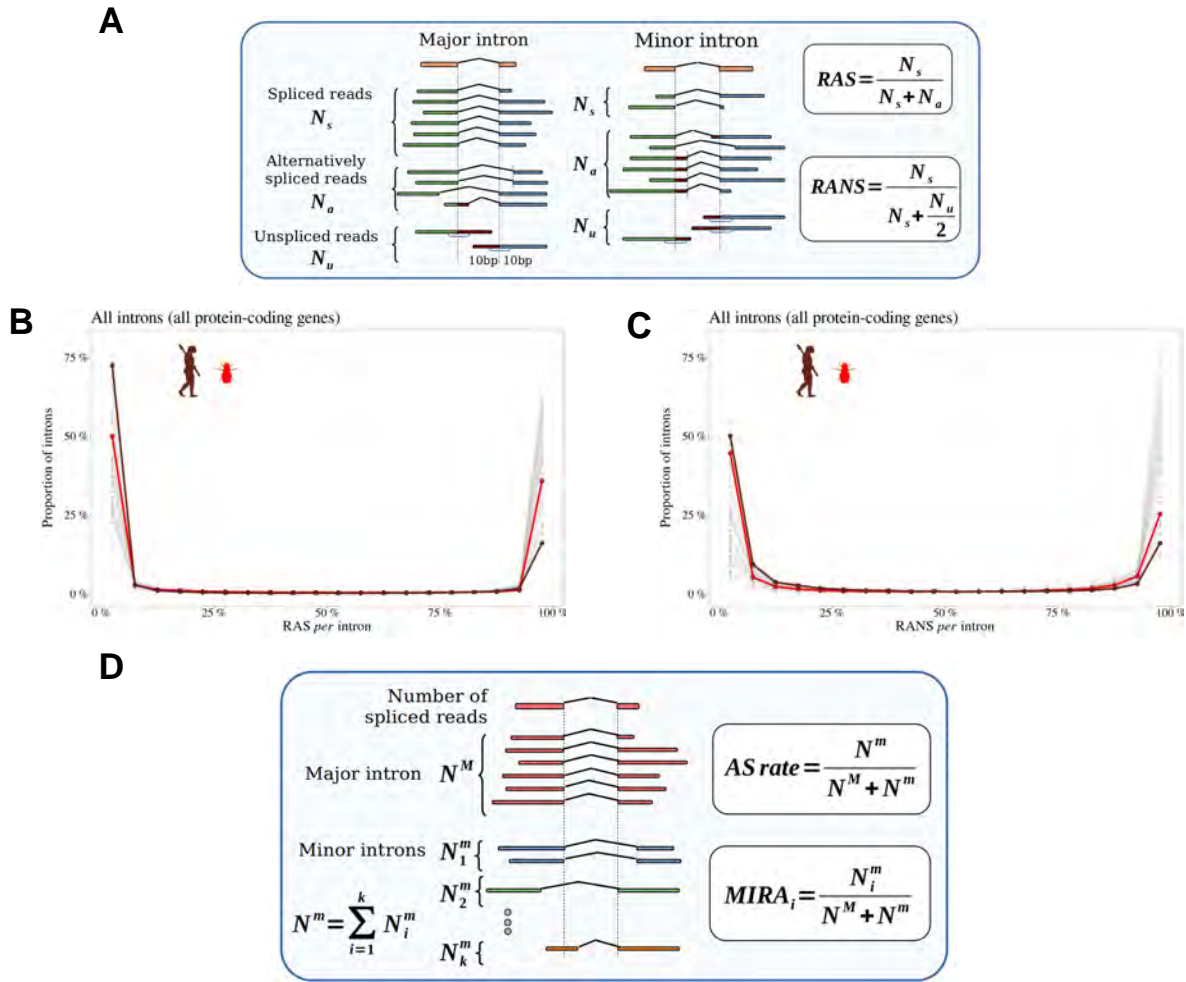


Figure 2: **Distinguishing major and minor introns.** **A:** Definition of the variables used to compute the relative abundance of the spliced isoform compared to other transcripts with alternative splice boundaries (RAS) or compared to unspliced transcripts (RANS): N_s : number of spliced reads corresponding to the precise excision of the focal intron; N_a : number of reads corresponding to alternative splice variants relative to this intron (*i.e.* sharing only one of the two intron boundaries); N_u : number of unspliced reads, co-linear with the genomic sequence. **B,C** Histograms representing the distribution of RAS and RANS values (divided into 5% bins), for protein-coding gene introns. Each line represents one species. Two representative species are colored: *Drosophila melanogaster* (red), *Homo sapiens* (brown). **D:** Description of the variables used to compute AS rate and minor intron relative abundance (MIRA), given a major intron: N^M : number of spliced reads corresponding to the excision of the major intron; N_i^m : number of spliced reads corresponding to the excision of a minor intron (i); N^m : total number of spliced reads corresponding to the excision of minor introns.

142 computed the rate of alternative splicing with respect to introns of the major isoform. We will hereafter use
 143 the term ‘splice variant’ (SV) to refer to those splicing events that are detected in a minority of transcripts
 144 (*i.e.* with $RAS \leq 0.5$ or $RANS \leq 0.5$).

145 We focused our analyses on **major** introns interrupting protein-coding regions (*i.e.* we excluded introns
 146 located within UTRs, [Materials & Methods](#)). In vertebrates, each BUSCO gene contains on average 8.4
 147 **major introns** ([Supplementary Tab. 1](#)). The intron density is more variable among insect clades, ranging
 148 from 2.8 **major** introns *per* BUSCO gene in Diptera to 6.1 in Blattodea. As expected, most major introns
 149 have GT/AG splice sites (99.1% on average across species), and only a small fraction have non-canonical
 150 boundaries (0.8% GC/AG and 0.1% AT/AC). The fraction of non-canonical splice sites is slightly higher
 151 among minor introns (2.8% GC/AG and 0.3% AT/AC). This might reflect a true biological difference but
 152 might also be caused by the presence of some false positives in the set of minor introns. In any case, the
 153 difference in splice signal usage between minor and major introns is small, which indicates that the vast
 154 majority of detected minor introns correspond to *bona fide* splicing events.

155 The proportion of major introns for which AS has been detected (*i.e.* with $N_a > 0$) ranges from 16.8% to
 156 95.7% depending on the species ([Supplementary Tab. 1](#)). This metric is however not very meaningful because
 157 it directly reflects differences in sequencing depth across species (the higher the sequencing effort, the higher
 158 the probability to detect a rare SV, [Supplementary Fig. 2](#)). To allow a comparison across taxa, we computed
 159 the AS **rate** of introns, normalized by sequencing depth ($AS = \frac{N_a}{N_s + N_a}$, [Materials & Methods](#)). The average
 160 AS rate for BUSCO genes varies by a factor of 5 among species, from 0.8% in *Drosophila grimshawi* (Diptera)
 161 to 3.8% in *Megachile rotundata* (Hymenoptera) (3.4% in humans). Interestingly, the average AS rates of
 162 BUSCO gene introns are significantly correlated with the three proxies of N_e : species longevity ([Fig. 3A](#)),
 163 body length and the dN/dS ratio ([Supplementary Fig. 3A,B](#)). These correlations are positive, which implies
 164 that AS rates tend to increase when N_e decreases. It is noteworthy that despite the fact that these proxies
 165 are not strongly correlated with each other ([Fig. 1B,C](#)), they all show similar relationships with AS rates.
 166 Thus, these observations are consistent with the hypothesis that N_e has an impact on the evolution of AS
 167 rate.

168 One limitation of our analyses is that we used heterogeneous sources of transcriptomic data. To obtain enough
 169 sequencing depth, we combined for each species many RNA-seq samples, irrespective of their origin (whole
 170 body, or specific tissues or organs, in adults or embryos, etc.). It is known that genome-wide average AS
 171 rates vary according to tissues or developmental stages ([Barbosa-Morais et al., 2012](#); [Mazin et al., 2021](#)), and
 172 according to environmental conditions ([John et al., 2021](#)). To explore how this might have affected our results,
 173 we repeated our analyses using a recently published dataset that aimed to compare transcriptomes across seven
 174 organs, sampled at several developmental stages in seven species (six mammals, one bird) ([Cardoso-Moreira
 175 et al., 2019](#)). In agreement with previous reports ([Mazin et al., 2021](#)), our analysis of BUSCO genes revealed
 176 substantial differences in AS rates among organs, with consistent patterns of variation across species. For
 177 instance, in all species, testes and brain tissues show higher AS rates than liver and kidney ([Fig. 3B](#)). However,
 178 the variation in AS rate among organs in each species is limited compared to differences in AS rate among
 179 species. Specifically, in an ANOVA analysis performed on the average AS rate across BUSCO gene introns,
 180 with the species and the organ of origin as explanatory variables, the species factor explained 89% of the total
 181 variance, while the organ factor explained only 9%. **Among insects, we found only one species (*Dendroctonus
 182 ponderosae*) for which RNA-seq samples were available from multiple tissues. Here again, the variance in AS
 183 rate among tissues was limited compared to inter-species variability** ([Supplementary Fig. 9](#)). Thus, despite

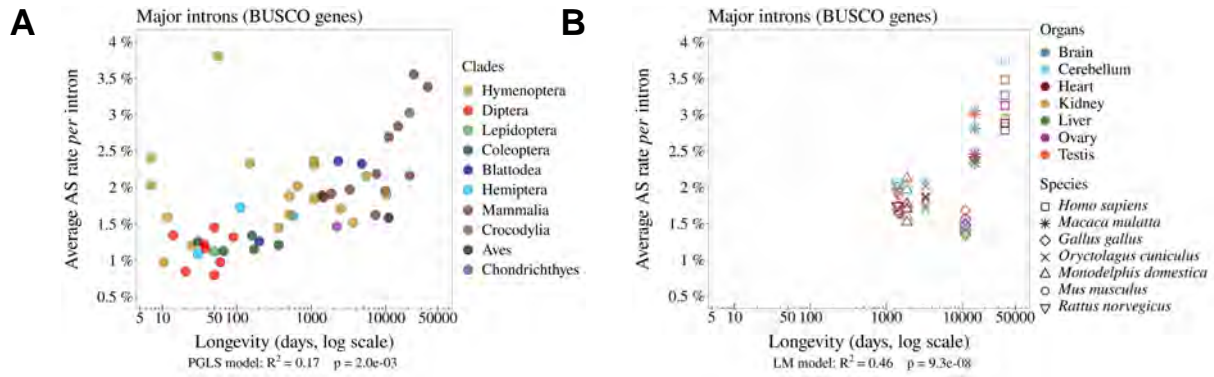


Figure 3: **The rate of alternative splicing correlates with life history traits across metazoans.** **A:** Relationship between the *per* intron average AS rate of an organism and its longevity (days, log scale). **B:** Variation in average AS rate across seven organs (brain, cerebellum, heart, liver, kidney, testis and ovary) among seven vertebrate species (RNA-seq data from Cardoso-Moreira *et al.* (2019)). AS rates are computed on major introns from BUSCO genes (Materials & Methods).

184 the variability that can be introduced by the heterogeneity of RNA-seq samples, the relationship between AS
 185 rate and longevity remains detectable among these seven species (Fig. 3B).

186 **Functional vs. non-functional alternative splicing**

187 The negative correlation observed between N_e and alternative splicing rates is consistent with the hypothesis
 188 that differences in AS rates across species are driven by variation in the rate of splicing errors (drift barrier
 189 model). This does not exclude however that functional splicing variants might also contribute to AS rate
 190 variation across species. To evaluate this point, we selected a subset of SVs that are enriched in functional
 191 AS events. To do this, we reasoned that selective pressure against the waste of resources should maintain
 192 splicing errors at a low rate (as low as permitted by the drift barrier), whereas functional SVs are expected to
 193 represent a sizeable fraction of the transcripts expressed by a given gene, at least in some specific conditions
 194 (cell type, developmental stage. . .). Thus, functional SVs are expected to be enriched among abundant SVs
 195 compared to rare SVs.

196 To assess this prediction, we analyzed the proportion of SVs that preserve the reading frame according
 197 to their abundance relative to the major isoform. For this, we focused on minor introns that share a
 198 boundary with one major intron and that have their other boundary at less than 30 bp from the major
 199 splice site (either in the flanking exon or within the major intron). We determined whether the distance
 200 between the minor intron boundary and the major intron boundary was a multiple of 3. We computed the
 201 abundance of **each** minor isoform, relative to the corresponding major isoform, with the following formula:
 202 **Minor intron relative abundance** $MIRA_1 = \frac{N_i^m}{N^m + N^m}$ (see Fig. 2D).

203 We divided minor introns into 5% bins according to their MIRA and computed for each bin the proportion of
 204 minor introns that maintain the reading frame of the major isoform (Fig. 4A). In all species, we observe
 205 that this proportion varies according to the abundance of splice variants, with two distinct regimes (Fig.
 206 4A). First, for MIRA values above 5%, the proportion of frame-preserving variants correlates positively with

207 MIRA, reaching up to 60%-70% for the most abundant isoforms. Second, for MIRA values below 1%, the
 208 proportion of frame-preserving variants does not covary with MIRA, and fluctuates around 30 to 40%, close
 209 to the random expectation (33%). The excess of frame-preserving variants among the most abundant isoforms
 210 implies that a substantial fraction of them is under constraint to encode functional protein isoforms. This
 211 fraction varies from 0% for MIRA values below 1%, to 50% for isoforms with the highest MIRA values. It
 212 should be noted that these estimates correspond to a lower bound, since it is possible that some frame-shifting
 213 splice variants are functional. Nevertheless, these observations clearly indicate that the subset of SVs with
 214 MIRA values $> 5\%$ (hereafter referred to as ‘abundant SVs’) is strongly enriched in functional isoforms relative
 215 to other SVs (MIRA $\leq 5\%$, hereafter referred to as ‘rare SVs’). Of note, the subset of rare SVs represents the
 216 vast majority of the SV repertoire (from 62.4% to 96.9% depending on the species; [Supplementary Tab. 1](#)).

217 Investigating selective pressures on minor splice sites

218 A complementary approach to assess the functionality of AS events consists in investigating signatures of
 219 selective constraints on splice sites. For this, we used polymorphism data from *Drosophila melanogaster*
 220 and *Homo sapiens* to measure single-nucleotide polymorphism (SNP) density at major and minor splice
 221 sites, considering separately rare and abundant SVs. We focused on the first two and last two bases of
 222 each intron (consensus sequences GT, AG), which represent the most constrained sites within splice signals.
 223 We studied minor introns that share one splice site with a major intron and we measured SNP density at
 224 the corresponding major and minor splice sites. To account for constraints acting on coding regions, we
 225 considered separately minor splice sites that were located in an exon or in an intron of the major isoform.
 226 As negative controls, we selected AG or GT dinucleotides that were unlikely to correspond to alternative
 227 splice sites ([Fig. 5, Materials & Methods](#)). Furthermore, for *Homo sapiens* we controlled for the presence of
 228 hypermutable CpG dinucleotides ([Tomso and Bell, 2003](#)) ([Supplementary Fig. 4, Materials & Methods](#)).

229 For both species, the lowest SNP density is observed at major splice signals, which reflects the strong selective
 230 constraints on these sites ([Fig. 5](#)). In *Drosophila melanogaster*, there is also a strong signature of selection on
 231 minor splice signals of abundant SVs: both in introns and in exons, the SNP density at minor splice signals
 232 of abundant SVs is much lower than in corresponding controls ([from -37% to -74%, Fig. 5A](#)) and than in
 233 minor splice signals of rare SVs ([from -38% to -71%, Fig. 5B](#)). This observation confirms that abundant SVs
 234 are strongly enriched in functional variants compared to rare SVs. In *Homo sapiens*, patterns of SNP density
 235 showed little evidence of selective constraints on minor splice sites, irrespective of the abundance of SVs ([Fig.](#)
 236 [5C,D](#)): minor acceptor splice sites (AG) located within the major intron show a weak but significant SNP
 237 deficit relative to corresponding control sites ([p-value \$< 1 \times 10^{-5}\$](#)), but other categories of minor splice sites do
 238 not show any sign of selective constraints. The fact that the signature of selection on minor splice signals is
 239 much weaker in humans compared to *Drosophila* [is indicative of](#) a lower prevalence of functional variants,
 240 even among abundant SVs. [This observation is therefore in total contradiction with the adaptive hypothesis](#)
 241 [\(more functional alternative splicing in complex organisms\).](#)

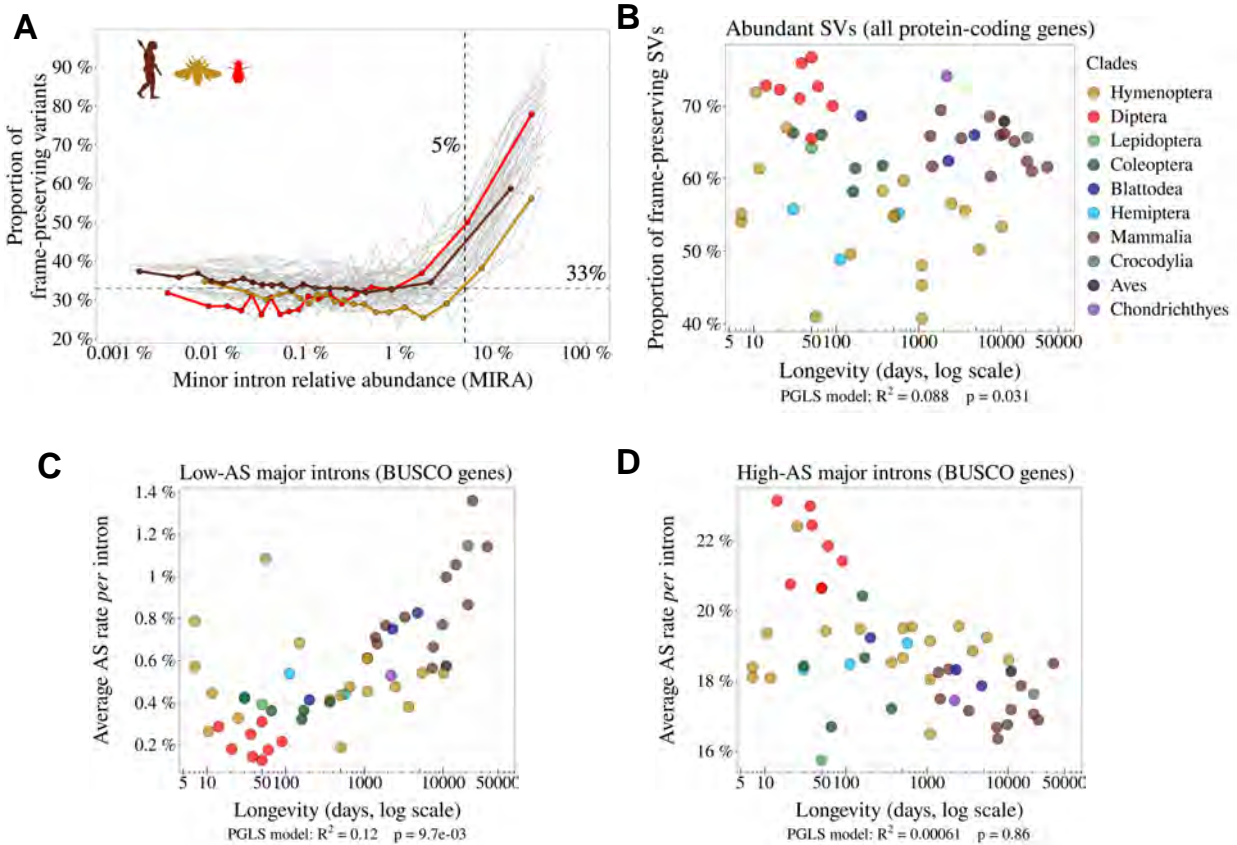


Figure 4: **Variation in AS rate across metazoans: distinguishing abundant splice variants (enriched in functional variants) from rare splice variants.** **A:** Frame-preserving isoforms are strongly enriched among abundant splice variants (SVs). For each species, SVs were classified into 20 equal-size bins according to their abundance relative to the major isoform (MIRA, see [Materials & Methods](#)), and the proportion of frame-preserving SVs was computed for each bin. Each line represents one species. Three representative species are colored: red: *Drosophila melanogaster*, brown: *Homo sapiens*, yellow: *Apis mellifera*. We used a threshold MIRA value of 5% to define ‘abundant’ vs. ‘rare’ SVs. **B:** Proportion of frame-preserving SVs among abundant SVs across metazoans. Each dot represents one species. All annotated protein-coding genes are used in the analysis. **C,D:** Relationship between the average *per* intron AS rate of an organism and its longevity (days, **log scale**). Only BUSCO genes are used in the analysis. **C:** Low-AS major introns (*i.e.* major introns that do not have any abundant SV), **D:** High-AS major introns (*i.e.* major introns having at least one abundant SV).

242 The splicing rate of rare SVs is negatively correlated with gene expression levels

243 The above analyses are consistent with the hypothesis that the vast majority of rare SVs correspond to
 244 erroneous transcripts, and that changes in N_e contribute to variation in AS rate across taxa by shifting the
 245 selection-mutation-drift balance. If true, then this model predicts that the erroneous AS rate should also vary
 246 among genes, according to their expression level. Indeed, it has been shown that the selective pressure on
 247 splicing accuracy is stronger on highly expressed genes (Saudemont *et al.*, 2017). This reflects the fact that for
 248 a given splicing error rate, the waste of resources (both in terms of metabolic cost and of futile mobilization

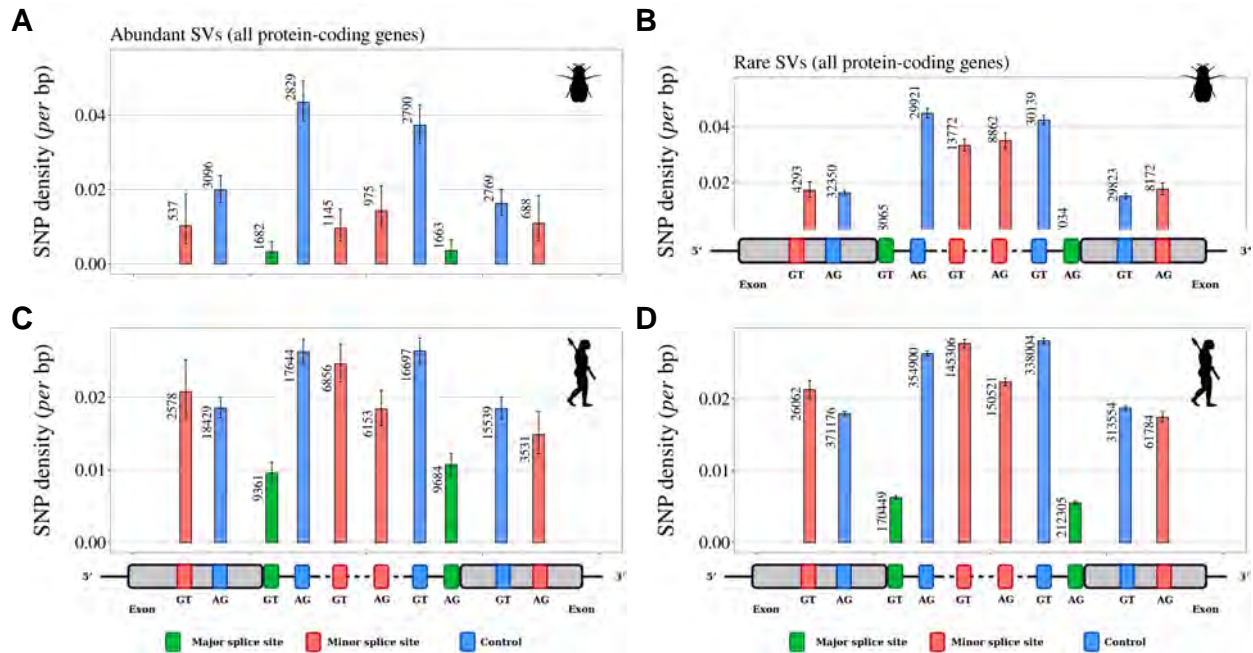


Figure 5: **Variation in selective constraints on alternative splice signals from rare and abundant SVs.** For each minor intron sharing one boundary with a major intron, we measured the SNP density at its minor splice site (red), and at the corresponding major splice site (green). We distinguished minor splice sites that are located in an exon or in an intron of the major isoform. As a control (blue), we selected AG or GT dinucleotides that are unlikely to correspond to alternative splice sites, namely: AG dinucleotides located toward the end of the upstream exon or the beginning of the intron (unlikely to correspond to a genuine acceptor site), and GT dinucleotides located toward the beginning of the downstream exon or the end of the intron (unlikely to correspond to a donor site). To increase the sample size, we analyzed data from all annotated protein-coding genes (and not only the BUSCO gene set). The number of sites studied is shown at the top of each bar. Error bars represent the 95% confidence interval of the proportion of polymorphic sites (proportion test). **A,B:** SNP density in *Drosophila melanogaster* (polymorphism data from 205 inbred lines derived from natural populations, $N=3,963,397$ SNPs (Huang *et al.*, 2014; Mackay *et al.*, 2012)). **C,D:** SNP density in *Homo sapiens* (polymorphism data from 2,504 individuals, $N=80,868,061$ SNPs (Auton *et al.*, 2015)). We excluded dinucleotides affected by CpG hypermutability (Materials & Methods, see Supplementary Fig. 4 for CpG sites). **A,C:** Abundant SVs (MIRA > 5%). **B,D:** Rare SVs (MIRA \leq 5%).

249 of cellular machineries) increases with gene expression level (Saudemont *et al.*, 2017; Xiong *et al.*, 2017).
 250 Thus, the selection-mutation-drift balance should lead to a negative correlation between gene expression level
 251 and the rate of splicing errors. To test this prediction, we focused on low-AS major introns, *i.e.* introns
 252 that are unlikely to have functional SVs. For each species, we considered all major introns with a sufficient
 253 sequencing depth to have a precise measure of their AS rate ($N_s + N_a \geq 100$). The selected subset represents
 254 38.1% to 86.7% of major introns of each species (median=70.9%). Introns were then divided into 20 bins of
 255 equal size, according to the expression level of the corresponding genes. For each species, we computed the
 256 Pearson correlation between the average AS rate and the average expression level across bins. We observed a
 257 negative correlation between AS rates and gene expression levels in 52 out of the 53 species (significant with

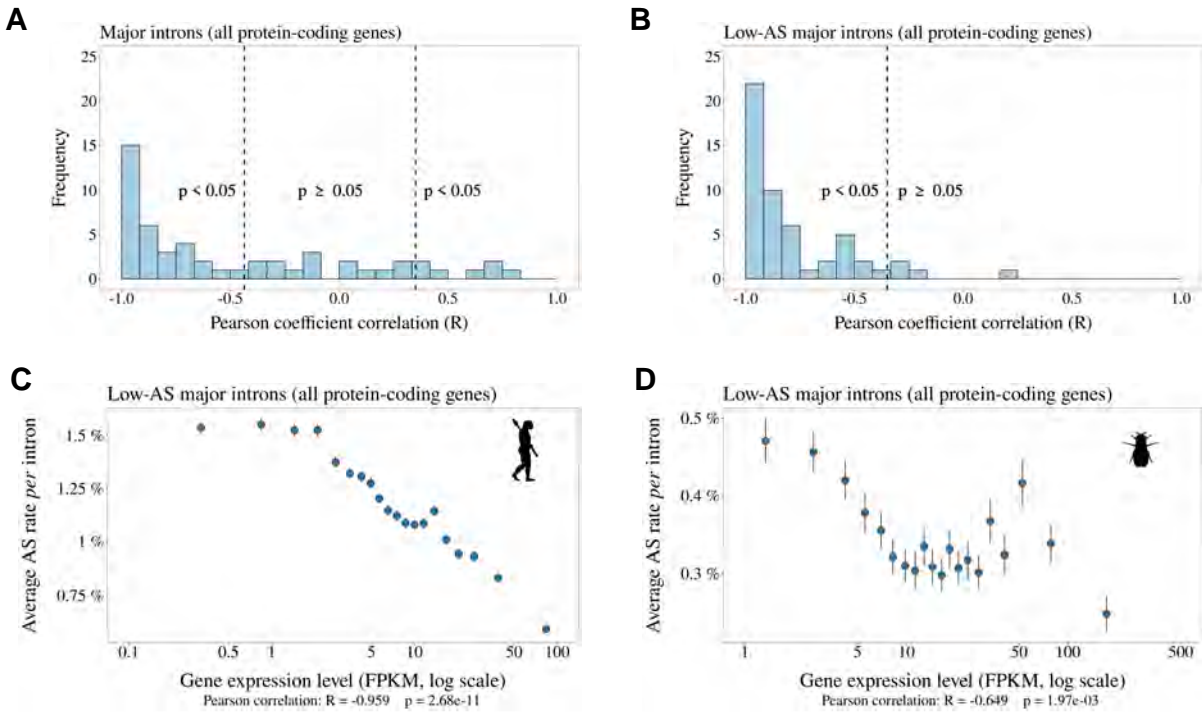


Figure 6: **Relationship between AS rate and gene expression level.** For each species, we selected major introns with a sufficient sequencing depth to have a precise measure of their AS rate ($N_s + N_a \geq 100$). We divided major introns into 5% bins according to their gene expression level and computed the correlation between the average AS rate and median expression level across the 20 bins. To increase sample size, these analyses were based on all annotated protein-coding genes (and not only the BUSCO gene set). **A**: Distribution of Pearson correlation coefficients (R) between the AS rate and expression level observed in the 53 metazoans. The vertical dashed lines indicates the thresholds under and above which correlations are significant (*i.e.* p -value < 0.05). **B**: Distribution of Pearson correlation coefficients computed **on the subsets of low-AS major introns** (*i.e.* after excluding major introns with abundant SVs). **C,D**: Two representative species illustrating the negative relation between the average AS rate of low-AS major introns and the expression level of their gene. Error bars represent the standard error of the mean. **C**: $N=127,599$ low-AS major introns from *Homo sapiens*, **D**: $N=31,357$ low-AS major introns from *Drosophila melanogaster*.

258 $p < 0.05$, in 48/53 species; Fig. 6B; two representative examples are shown in Fig. 6C and 6D). This pattern
 259 indicates that in almost all metazoan species, genes with a higher expression level have a lower AS rate,
 260 consistent with the hypothesis the rate of splicing errors is shaped by the selection-mutation-drift balance. It
 261 should be noted that this negative correlation between AS rate and gene expression level is not expected for
 262 functional SVs (there is *a priori* no reason why the AS rate of functional SVs should be higher in weakly
 263 expressed genes than in highly expressed genes). Interestingly, when we performed this analysis on all introns
 264 (including those with abundant SVs, which are enriched in functional variants), then most species (31/53)
 265 still showed a negative correlation between AS rate and gene expression level (Fig. 6A), but some species,
 266 such as *Drosophila melanogaster* showed the opposite pattern (Supplementary Fig. 5). This probably reflects

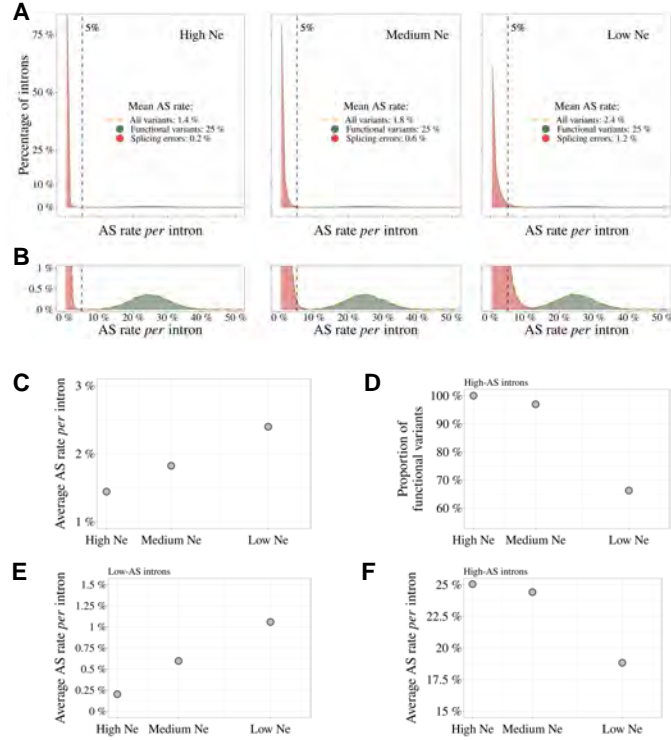


Figure 7: **Impact of the drift-barrier on the genome-wide AS rate: model predictions.** To illustrate the impact of the drift barrier, we sketched a simple model, with three hypothetical species of different N_e . In this model, the repertoire of SVs consists of a mixture of functional variants and splicing errors. We assumed that in all species, only a small fraction of **major** introns (5%) produce functional SVs, but that these variants have a relatively high AS rate (average=25%, standard deviation=5%; see [Materials & Methods](#) for details on model settings). Splicing error rates were assumed to be gamma-distributed, with a low mean value. Owing to the drift barrier effect, the mean error rate was set to vary from 0.2% in species of high N_e to 1.2% in species of low N_e (these parameters were chosen to match approximately the AS rates observed in empirical data for rare SVs). **A** Genome-wide distribution of AS rates in each species (high N_e , medium N_e and low N_e). Each distribution corresponds to a mixture of functional SVs (green) and splicing errors (red). **B**: Zoom on the y-axis to better visualize the contribution of functional SVs to the whole distribution: rare SVs ($AS \leq 5\%$) essentially correspond to splicing errors, while abundant SVs ($AS > 5\%$) correspond to a mixture of functional and spurious variants, whose relative proportion depend on N_e . The following panels show how these different distributions, induced by differences in N_e , impact genome-wide AS patterns. **C**: Relationship between the average AS rate *per major* intron and N_e . **D**: Fraction of frame-preserving **splice** variants among introns with high AS rates *vs* N_e . Relationship between the average AS rate *per* intron and N_e , for ‘low-AS’ major introns ($MIRA \leq 5\%$) (**E**), and for ‘high-AS’ major introns ($MIRA > 5\%$) (**F**).

267 that fact that, in those species, functional AS events make a significant contribution to the genome-wide
 268 average AS rate.

269 **Discussion**

270 To investigate the factors that drive variation in AS rates across species, we analyzed publicly available
 271 RNA-seq data across a large set of 53 species, from diverse metazoan clades, covering a wide range of N_e values.
 272 To facilitate comparisons across species, we sought to limit the impact of the among-gene variance in AS rates.
 273 For this, we primarily based our analyses on a common set of nearly 1,000 orthologous protein-coding genes
 274 (BUSCO gene set). We focused our study on introns located within protein-coding regions, because introns
 275 from UTRs or lncRNAs are expected to be subject to different functional constraints. We measured AS rates
 276 on introns corresponding to a major isoform. When sequencing depth is limited, the set of introns for which
 277 AS can be quantified is biased toward the most highly expressed genes. To avoid this bias, we restricted our
 278 study to species for which the median sequencing depth of BUSCO exons was above 200. With this setting,
 279 on average 96.9% of BUSCO annotated introns could be analyzed in each species (Supplementary Tab. 1).

280 We observed a 5-fold variation in the average AS rate of BUSCO introns across species from 0.8% in *Drosophila*
 281 *grimshawi* (Diptera) to 3.8% in *Megachile rotundata* (Hymenoptera) (Fig. 3A). In agreement with previous
 282 work, we observed that AS rates tend to be high in vertebrates (average=2.3%), and notably in primates
 283 (average=3.1%) (Barbosa-Morais *et al.*, 2012; Chen *et al.*, 2014; Mazin *et al.*, 2021). This observation was
 284 previously interpreted as an evidence that AS played an important role in the diversification of the functional
 285 repertoire necessary for the development of more complex organisms (Chen *et al.*, 2014). However, this
 286 pattern is also compatible with the hypothesis that variation in AS rates across species result from differences
 287 in splicing error rates, which are expected to be higher in species with low N_e (Bush *et al.*, 2017). Indeed,
 288 consistent with this drift barrier hypothesis, we observed significant correlations between AS rates and proxies
 289 of N_e (Fig. 3B, Supplementary Fig. 3A,B).

290 In their original study, (Chen *et al.*, 2014) investigated the hypothesis that variation in AS rates across taxa
 291 might be driven by variation in N_e . For this, they focused on 12 species, for which they had measured levels
 292 of polymorphism at silent sites (π). They found that the correlation between AS rate and the number of
 293 cell types (proxy for organismal complexity) remained significant after controlling for π . They therefore
 294 concluded that the association between the cellular diversity and alternative splicing was not a by-product
 295 of reduced effective population sizes among more complex species. This conclusion was however based on
 296 a very small sample of species. More importantly, it assumed that π could be taken as a proxy for N_e . At
 297 mutation-drift equilibrium, π is expected to be proportional to $N_e u$ (where u is the mutation rate *per* bp
 298 *per* generation). Thus, if u is constant across taxa, π can be used to estimate variation in N_e . However, the
 299 dataset analyzed by Chen *et al.* (2014) included very diverse eukaryotic species, with mutation rates ranging
 300 from 1.7×10^{10} mutation *per* bp *per* generation in budding yeast, to 1.1×10^8 mutation *per* bp *per* generation in
 301 humans (Lynch *et al.*, 2016). Hence, at this evolutionary scale, variation in N_e cannot be directly inferred
 302 from π without accounting for variation in u . Moreover, the drift barrier hypothesis states that the AS rate
 303 of a species should reflect the genome-wide burden of slightly deleterious substitutions, which is expected to
 304 depend on the intensity of drift over long evolutionary times (*i.e.* long-term N_e). Conversely, π reflects N_e
 305 over a short period of time (of the order of N_e generations), and can be strongly affected by recent population
 306 bottlenecks (too recent to have substantially impacted the genome-wide deleterious substitution load). The

307 drift barrier hypothesis therefore predicts that the splicing error rate should correlate more strongly with
 308 proxies of long-term N_e (such as dN/dS , life history traits, or organismal complexity) than with π . The fact
 309 that AS rates remained significantly correlated to cellular diversity after controlling for π (Chen *et al.*, 2014)
 310 is therefore not a conclusive argument against the drift barrier hypothesis.

311 To contrast the two models (drift barrier vs diversification of the functional repertoire in complex organisms),
 312 we sought to distinguish functional splice isoforms from erroneous splicing events. Based on the assumption
 313 that splicing errors should occur at a low frequency, we split major introns into two categories, those with
 314 abundant SVs (MIRA > 5%), and those without (MIRA \leq 5%). Rare SVs represent the vast majority of
 315 the repertoire of splicing isoforms detected in a given transcriptome (from 62.4% to 96.9% according to the
 316 species; Supplementary Tab. 1). Two lines of evidence indicate that the small subset of abundant isoforms is
 317 strongly enriched in functional transcripts relative to other SVs. First, we observed that in all species, the
 318 proportion of SVs that preserve the reading frame is much higher among abundant SVs than among rare
 319 SVs (Fig. 4A). Second, the analysis of polymorphism data in *Drosophila* indicates that the average level of
 320 purifying selection on alternative splice sites is much stronger for abundant than rare SVs (Fig. 5A,B).

321 If variation in AS rate across species had been driven by a higher prevalence of functional SVs in more complex
 322 organisms, one would have expected the proportion of frame-preserving SVs to be stronger in vertebrates
 323 than in insects, in particular for the set of introns with high AS rate (*i.e.* enriched in functional SVs). On
 324 the contrary, the highest proportion of frame-preserving SVs is observed in dipterans (Fig. 4B). In fact, the
 325 overall higher AS rate of vertebrates (Fig. 3A) is driven by the set of introns with a low AS rate (Fig. 4C),
 326 *i.e.* the set of introns in which the prevalence of functional SVs is the lowest. On the contrary, among the set
 327 of introns with high AS rate, vertebrates have lower AS rates than insects (Fig. 4D).

328 These observations are difficult to reconcile with the hypothesis that the higher AS rate in vertebrates results
 329 from a higher rate of functional AS. Conversely, these observations fit very well with a model where variation
 330 in AS rate across species is entirely driven by variation in the efficacy of selection against splicing errors. To
 331 illustrate this model, let us consider three hypothetical species with different N_e , in which a small fraction of
 332 major introns (say 5%) is subject to functional alternative splicing. Let us consider that the distribution of
 333 AS rates of functional splicing variants is the same for all species (*i.e.* independent of N_e), with a mean of
 334 25% (and a standard deviation of 5%). In addition, we assume that all major introns are potentially affected
 335 by splicing errors, with a mean error rate ranging from 0.2% in species of high N_e to 1.2% in species of
 336 low N_e , owing to the drift barrier effect (these parameters were set to match approximately the AS rates
 337 observed in empirical data for rare SVs). The distributions of AS rate given by this model are presented
 338 in Fig. 7A: rare SVs (MIRA \leq 5%) essentially correspond to splicing errors, while abundant SVs (MIRA
 339 > 5%) correspond to a mixture of functional and spurious variants, whose relative proportion depend on
 340 N_e (Fig. 7B). Interestingly, the predictions of this simple model fit remarkably well with our observations:
 341 we observed a positive correlation between AS rate and longevity (*i.e.* a negative correlation with N_e) for
 342 the set of low-AS major introns (Fig. 4C), but an opposite trend for high-AS major introns (Fig. 4D), as
 343 predicted by the model (Fig. 7D,E). Given that high-AS major introns represent only a small fraction of

344 **major** introns, this model predicts that, overall, AS rates correlate negatively with N_e (Fig. 7), as observed
 345 in empirical data (Fig. 3A, Supplementary Fig. 3).

346 It should be noted that the BUSCO dataset corresponds to genes that are strongly conserved across species,
 347 often highly expressed, and hence might not be representative of the entire genome. Notably, AS rates are on
 348 average lower in the BUSCO gene set than in other genes, even after accounting for their expression level
 349 (Supplementary Fig. 5). However, results remained qualitatively unchanged when we repeated our analyses
 350 on the whole set of annotated protein-coding genes for each species: correlations between AS rates and N_e
 351 proxies are slightly weaker than on the BUSCO subset, but remain significant (Supplementary Fig. 6).

352 The model also predicts that the proportion of functional SVs among high-AS major introns should vary with
 353 N_e (Fig. 7C). To assess this point, we measured in each species the enrichment in reading frame-preserving
 354 events among abundant SVs compared to rare SVs. As predicted, this estimate of the prevalence of functional
 355 SVs tends to decrease with decreasing N_e proxies (*e.g.* Fig. 3A, where N_e is approximated by longevity).
 356 However, these correlations are weak, marginally significant after accounting for phylogenetic inertia with
 357 only two of the three N_e proxies, and not robust to multiple testing issues (Supplementary Fig. 7). Thus, N_e
 358 does not appear to be a strong predictor of the prevalence of functional SVs among high-AS major introns.

359 According to the drift-barrier model, the level of splicing errors is expected to decrease with increasing
 360 selective pressure. In all above analyses, we considered AS rates measured *per* intron, and not *per* gene. Yet,
 361 the trait under selection is the *per*-gene error rate, which depends not only on the error rate *per* intron,
 362 but also on the number of introns *per* gene. Given that intron density varies widely across clades (from 2.8
 363 introns *per* gene in diptera to 8.4 introns *per* gene in vertebrates; Supplementary Tab. 1), the correlations
 364 reported above between AS rates and N_e may undervalue the predictive power of the drift-barrier model. The
 365 RNA-seq datasets that we analyzed consist of short-read sequences, which do not allow a direct quantification
 366 of the *per*-gene AS rate. We therefore indirectly estimated the *per*-gene AS rate in each species, based on the
 367 *per*-intron AS rate and on the number of introns *per* gene (Materials & Methods). Interestingly, as predicted
 368 by the drift-barrier model, N_e proxies correlate more strongly with this estimate of the *per*-gene AS than
 369 with the *per*-intron AS rates (Supplementary Fig. 8).

370 One other important prediction of the drift barrier model is that splicing error rate should vary not only
 371 across species according to N_e , but also among genes, according to their expression level. Indeed, for a given
 372 splicing error rate, the waste of resources (and hence the fitness cost) is expected to increase with the level of
 373 transcription. Thus, the selective pressure for optimal splice signals is expected to be higher, and hence the
 374 error rate to be lower, in highly expressed genes. Consistent with that prediction, nearly all species show a
 375 negative correlation between gene expression level and AS rate in low-AS major introns (Fig. 6C).

376 It should be noted that our analyses suffer from several important limitations. First, the proxies that we
 377 considered for N_e are quite noisy (Fig. 1). Second, to maximize the number of species in our analyses, we
 378 had to use very heterogeneous sources of RNA (whole-body, specific tissues, or organs, at different life stages,
 379 in different sexes, different environmental conditions, etc.). Third, we used short-read sequencing data, which
 380 allow the quantification of AS rates for individual introns, but do not provide a direct measure of AS rates
 381 *per* gene. **Hopefully progress of long-read sequencing technologies will soon allow the comparative analysis of**

382 AS rates on full-length transcripts (*e.g.* see Leung *et al.* (2021)). But presently, publicly available long-read
 383 transcriptomic data are restricted to a narrow set of model organisms, and their sequencing depth is still too
 384 limited to quantify rare splicing events. The fact that we detected significant correlations between AS rate
 385 and the three N_e proxies, despite these uncontrolled sources of variability, suggests that we underestimate
 386 the effect of N_e on AS rates.

387 Thus, overall, all observations fit qualitatively well with the predictions of the drift barrier model, according
 388 to which most of the variation in AS rate across species reflects differences in splicing error rates. Of course,
 389 this model is not in contradiction with the fact, well established, that some AS events play an essential role
 390 in various processes. Different criteria can be used to distinguish functional SVs from spurious splicing events.
 391 Notably, AS events that are strongly tissue-specific or developmentally dynamic tend to be more conserved
 392 across species, which indicates that a substantial fraction of them are evolutionary constrained, and hence
 393 functional (Mudge *et al.*, 2011; Barbosa-Morais *et al.*, 2012; Merkin *et al.*, 2012; Reyes *et al.*, 2013). The
 394 abundance of a SV is also an important predictor of its functionality. In particular, we observed that in all
 395 species, the proportion of frame-preserving events is much higher among abundant SVs than among rare SVs
 396 (Fig. 4A). We note however that the threshold that we used to define abundant SVs is somewhat arbitrary.
 397 In fact, according to our model, this class of SVs corresponds to a mixture of functional and spurious events,
 398 whose relative proportion is expected to depend on N_e (Fig. 7C). Thus, in low- N_e species, even the subset of
 399 abundant SVs includes a substantial fraction of errors. This probably explains why, contrarily to *Drosophila*,
 400 we do not detect any signature of purifying selection on alternative splice signals in humans, even for abundant
 401 SVs (Fig. 5).

402 In conclusion, all observations fit with the hypothesis that random genetic drift sets an upper limit on the
 403 capacity of selection to prevent splicing errors. It should be noted that this limit on the optimization of
 404 genetic systems is expected to affect not only splicing, but all aspects of gene expression. Notably, there
 405 is a growing body of evidence that the complexity of transcripts produced by eukaryotic genes (resulting
 406 from alternative transcription initiation, polyadenylation, splicing or back-splicing, RNA editing) often does
 407 not correspond to fine-tuned adaptations but simply to the accumulation of errors (Pickrell *et al.*, 2010;
 408 Saudemont *et al.*, 2017; Xu *et al.*, 2019; Xu and Zhang, 2018; Liu and Zhang, 2018b,a; Xu and Zhang,
 409 2014, 2020; Gout *et al.*, 2013; Zhang and Xu, 2022). It should be noted however that the relationship
 410 between the genome-wide error rate and N_e is not expected to be monotonic. Indeed, models predict that
 411 in species with very high N_e , selection on each individual gene should favor genotypes that are robust
 412 to errors of the gene expression machinery, which in turn, reduces the constraints on the global level of
 413 gene expression errors (Rajon and Masel, 2011; Xiong *et al.*, 2017). Thus, paradoxically, species with very
 414 large N_e are expected to have gene expression machineries that are more error-prone than species with
 415 very small N_e (Rajon and Masel, 2011). This argument was developed by Xiong *et al.* (2017) to account
 416 for the fact that transcription error rates had been found to be about 10 times higher in bacteria than
 417 in eukaryotes (Traverse and Ochman, 2016; Gout *et al.*, 2013). More recent work indicates that bacterial
 418 transcription error rates had been largely overestimated, presumably owing to RNA damages during the
 419 preparation of sequencing libraries (Li and Lynch, 2020). Given these uncertainties in the measures of
 420 transcription error rates, it seems for now difficult to interpret the differences reported across species. But in

421 any case, it is important to note that it is in principle possible that the drift barrier affects differently the
422 different steps of the gene expression process. It would therefore be important to investigate to which extent
423 each step of gene expression responds (or not) to variation in N_e . As illustrated here by the relationship
424 observed between alternative splicing and N_e , it appears essential to consider the contribution of non-adaptive
425 evolutionary processes when trying to understand the origin of eukaryotic gene expression complexity.

426 **Materials & Methods**

427 **Genomic and transcriptomic data collection**

428 To analyze AS rate variation across metazoans, three types of information are required: transcriptome
429 sequencing (RNA-seq) datasets, genome assemblies, and gene annotations. To obtain this data, we first
430 queried the Short Read Archive database (Leinonen *et al.*, 2011) to extract publicly available RNA-seq datasets.
431 We also queried the NCBI Genomes database (NCBI Resource Coordinators, 2018) to retrieve genomic
432 sequences and annotations. When this project was initiated, the vast majority of metazoans represented in
433 this database corresponded to vertebrates or insects. We therefore decided to focus our analyses on these two
434 clades ($N=69$ species).

435 **Identification of orthologous gene families**

436 To be able to compare average AS rates across species, given that AS rates vary among genes (Saudeмонт
437 *et al.*, 2017), it is necessary to analyze a common set of orthologous genes. We searched for homologues of
438 the BUSCOv3 (Benchmarking Universal Single Copy Orthologs, (Seppey *et al.*, 2019)) metazoan gene subset
439 ($N=978$ genes) in each of the 69 genomes. To do this, we used the software BUSCO v.3.1.0 to associate
440 BUSCO genes to annotated protein sequences. For each species, BUSCO genes were removed from the
441 analysis if they were associated to more than one annotated gene or to an annotated gene that was associated
442 to more than one BUSCO gene.

443 **RNA-seq data processing and intron identification**

444 We aligned the RNA-seq reads on the corresponding reference genomes with HISAT2 v.2.1.0 (Kim *et al.*,
445 2019). We built the genome indexes using annotated introns and exons coordinates in addition to genome
446 sequences, to improve splice junction detection sensitivity. The maximum allowed intron length was fixed to
447 2,000,000 bp. We then extracted intron coordinates from HISAT2 alignments using an in-house perl script
448 that scanned for CIGAR strings containing N , which indicate regions that are skipped from the reference
449 sequence. For intron detection and quantification we used only uniquely mapping reads that had a maximum
450 mismatch ratio of 0.02. We required a minimum anchor length (that is, the number of bases that align on
451 each flanking exon) of 8 bp for intron detection, and of 5 bp for intron quantification. We kept only those
452 predicted introns that had GT-AG, GC-AG or AT-AC splice signals, and we predicted the strand of the
453 introns based on the splice signal.

454 We assigned an intron to a gene if at least one of the intron boundaries fell within 1 bp of the annotated
 455 exon coordinates of the gene, combined across all annotated isoforms. We excluded introns that could not
 456 be unambiguously assigned to a single gene. We distinguish annotated introns (which appear as such in
 457 the reference genome annotations) and un-annotated introns, which were detected with RNA-seq data and
 458 assigned to previously annotated genes.

459 We further restricted our analyses to introns located within protein-coding regions. To do this, for each
 460 protein-coding gene, we extracted the start codons and the stop codons for all annotated isoforms. We then
 461 identified the minimum start codon and the maximum end codon positions and we excluded introns that
 462 were upstream or downstream of these extreme coordinates.

463 **The alignment process, which is the most time-consuming step in the pipeline (see Supplementary Fig. 10),**
 464 **can take up to one week when using 16 cores *per* RNA-seq for larger genomes, such as mammals. Additionally,**
 465 **the processed compressed files generated during this process can exceed 7 terabytes in size.**

466 **Alternative splicing rate definition**

467 For each intron we noted N_s the number of reads corresponding to the precise excision of this intron (spliced
 468 reads), and N_a the number of **alternatively spliced reads** (*i.e.* **spliced variant** sharing only one of the two intron
 469 boundaries). Finally, we note N_u the number of unspliced reads, co-linear with the genomic sequence, and
 470 which overlap with at least 10 bp on each side of an exon-intron boundary. These definitions are illustrated in
 471 **Fig. 2**. We then defined the relative abundance of the focal intron compared to introns with one alternative
 472 splice boundary ($RAS = \frac{N_s}{N_s + N_a}$), as well as relative to unspliced reads ($RANS = \frac{N_s}{N_s + \frac{N_u}{2}}$).

473 To compute these ratios we required a minimal number of 10 reads at the denominator. We thus calculated
 474 the RAS only if $(N_s + N_a) \geq 10$ and the RANS only if $(N_s + \frac{N_u}{2}) \geq 10$ (**We divided N_u by 2 because retention**
 475 **is quantified at two sites, which increases the detection power by a factor of 2). If the criteria were not**
 476 **met, the values were labeled as not available (NA).** We computed these ratios using reads from all available
 477 RNA-seq samples, unless otherwise specified (for example, in sub-sampling analyses). Based on these ratios
 478 we defined three categories of introns: major introns, defined as those introns that have $RANS > 0.5$ and
 479 $RAS > 0.5$; minor introns, defined as those introns that have $RANS \leq 0.5$ or $RAS \leq 0.5$; unclassified introns,
 480 which **do not satisfy** the above conditions.

481 For minor introns sharing a boundary with a major intron, we computed the relative abundance
 482 of the minor intron (i) with respect to the corresponding major intron, with the following formula:
 483 **Minor intron relative abundance $MIRA_i = \frac{N_i^m}{N^M + N^m}$, where N^M is the number of spliced reads corresponding**
 484 **to the excision of the major intron, N_i^m is the number of spliced reads corresponding to the excision of a**
 485 **minor intron (i) and N^m is the total number of spliced reads corresponding to the excision of minor introns**
 486 **(see Fig. 2).**

487 We defined the *per-gene* AS rate as the probability to **observe** at least one alternative splicing event across all
 488 the major introns of **a gene**. **To estimate the per-gene AS rate of a given gene, we assumed that the AS rate is**
 489 **uniform across its major introns, and that AS events occur independently at each intron. We calculated the**
 490 **AS rate for each gene as the number of spliced reads corresponding to the excision of major introns, divided**

491 by the number of spliced reads corresponding to minor and major introns ($\frac{\sum N^m}{\sum N^M + N^m}$). The probability for
 492 a given gene to produce no splice variant across all its major introns is thus $p_0 = (1 - \frac{\sum N^m}{\sum N^M + N^m})^{N_i}$, where
 493 N_i is the number of major introns of the gene. The *per*-gene AS rate (ASg), i.e. the probability to have at
 494 least one AS event, is therefore the complement of p_0 : ASg=1- p_0 .

495 Identification of reading frame-preserving splice variants

496 To determine the proportion of open reading frame-preserving splice variants, we first identified minor introns
 497 that had their minor splice site within a maximum distance of 30 bp from the major splice site (either in
 498 the flanking exon or within the major intron). Among these introns, we considered that frame-preserving
 499 variants are those introns for which the distance between the minor intron boundary and the major intron
 500 boundary was a multiple of 3.

501 Gene expression level

502 Gene expression levels were calculated with Cufflinks v2.2.1 (Roberts *et al.*, 2011) based on the read alignments
 503 obtained with HISAT2, for each RNA-seq sample individually. We estimated FPKM levels (fragments *per*
 504 kilobase of exon *per* million mapped reads) for each gene.

505 The overall gene expression of a gene was computed as the average FPKM across samples, weighted by the
 506 sequencing depth of each sample. The sequencing depth of a sample is the median *per*-base read coverage
 507 across BUSCO genes.

508 Phylogenetic tree reconstruction

509 For each of the 978 BUSCO gene families we collected the longest corresponding proteins identified in each
 510 species. We removed proteins for which the amino acid sequence provided with the annotations did not
 511 perfectly correspond to the translation of the corresponding coding sequences. We then aligned the resulting
 512 sets of protein-coding sequences for each BUSCO gene, using the codon alignment option in PRANK v.170427
 513 (Löytynoja and Goldman, 2008). We translated the codon alignments into protein alignments using the R
 514 package seqinr (Charif and Lobry, 2007). To infer the phylogenetic tree rapidly, we sub-sampled the resulting
 515 multiple alignments ($N=461$), selecting alignments with the highest number of species (ranging from 49 to
 516 53 species *per* alignment). We then concatenated these alignments and kept sites that were aligned in at
 517 least 30 species. We used RAxML-NG v.0.9.0 (Kozlov *et al.*, 2019) to infer the species phylogeny with a final
 518 alignment of 53 taxa and 165,648 sites (amino acids). RAxML was set to perform one model *per* gene with
 519 fixed empirical substitution matrix (LG), empirical amino acid frequencies from alignment (F) and 8 discrete
 520 GAMMA categories (G8), specified in a partition file with one line *per* multiple alignment. The analysis
 521 generated 10 starting trees, 5 starting from a random topology and 5 starting from a tree generated by the
 522 parsimony-based randomized stepwise addition algorithm. The best-scoring topology was kept as the final
 523 ML tree and 10 bootstrap replicates have been generated.

524 ***dN/dS* computation**

525 We estimated *dN/dS* ratios for the BUSCO gene families that were present in at least 45 species (N=922 genes),
 526 using the codon alignments obtained with PRANK (see above). We divided the 922 sequence alignments into
 527 18 groups, based on their average GC3 content across species, and concatenated the alignments within each
 528 group. We thus obtained concatenated alignments that were 209 kb long on average. We used bio++ v.3.0.0
 529 libraries (Guéguen *et al.*, 2013; Dutheil and Boussau, 2008; Bolívar *et al.*, 2019) to estimate the *dN/dS* on
 530 terminal branches of the phylogenetic tree, for each concatenated alignment. We attributed the *dN/dS* of
 531 the terminal branches to the species that corresponds.

532 In a first step, we used an homogeneous codon model implemented in bppml to infer the most likely branch
 533 lengths, codon frequencies at the root, and substitution model parameters. We used YN98 (F3X4) (Yang
 534 and Nielsen, 1998) substitution model, which allows for different nucleotide content dynamics across codon
 535 positions. In a second step, we used the MapNH substitution mapping method (Guéguen and Duret, 2018)
 536 to count synonymous and non-synonymous substitutions (Dutheil *et al.*, 2012). We defined dN as the total
 537 number of non-synonymous substitutions divided by the total number of non-synonymous opportunities, both
 538 summed across concatenated alignments, for each branch of the phylogenetic tree. Likewise, we defined dS as
 539 the total number of synonymous substitutions divided by the total number of synonymous opportunities,
 540 both summed across concatenated alignments. The *per-species dN/dS* corresponds to the ratio between dN
 541 and dS, on the terminal branches of the phylogenetic tree.

542 **Life history traits**

543 We used various life history traits to approximate the effective population size of each species. For vertebrates
 544 species we considered the maximum lifespan (*i.e.* from birth to death) and body length referenced. For insects
 545 we took the maximum lifespan and body length of the *imago*. For eusocial insects and the eusocial mammal
 546 *Heterocephalus glaber*, the selected values correspond to the queens. The sources from which the lifespan and
 547 the body length information was taken are listed in [data/Data9-suppl.pdf](#) in the Zenodo repository (see
 548 [Data and code availability](#)).

549 **Analyses of sequence polymorphism**

550 We analyzed the distribution of single nucleotide polymorphisms (SNPs) around splice sites in *Drosophila*
 551 *melanogaster* and *Homo sapiens*.

552 For *Drosophila melanogaster* we used polymorphism data from the *Drosophila* Genetic Reference Panel
 553 (DGRP) (Huang *et al.*, 2014; Mackay *et al.*, 2012), from which we extracted 39,633,97 SNPs that
 554 were identified from comparisons across 205 inbred lines. We converted the SNP coordinates from
 555 the dm3 genome assembly to the dm6 assembly with the liftOver utility (Hinrichs *et al.*, 2006) of the
 556 UCSC genome browser, using a whole genome alignment between the two assemblies downloaded from
 557 [<https://hgdownload.soe.ucsc.edu/goldenPath/dm3/liftOver/dm3ToDm6.over.chain.gz>].

558 For *Homo sapiens* we used polymorphism data from the 1000 Genomes project, phase 3 release (Auton *et al.*,
559 2015). This dataset included 80,868,061 SNPs that were genotyped in 2,504 individuals.

560 For each minor intron sharing one boundary with a major intron, we computed the number of SNPs that
561 occur at their respective splice sites: at their shared boundary, and at the major intron and minor introns
562 specific boundaries.

563 We focused our study on minor introns that have their specific boundary folding in the exons adjacent to the
564 major intron or in the major intron. As a control, for each minor intron, we searched for one GT and one AG
565 dinucleotides in the interval between 20 and 60 bp with respect to the major splice site, in the neighboring
566 exon and in the **major** intron, and computed the number of SNPs that occur on these sites. We searched for
567 control AG dinucleotides in the **vicinity of the donor splice site of the major** intron and for GT dinucleotides
568 in the **vicinity of its acceptor splice site**, to avoid studying sites that might correspond to **unidentified** minor
569 splice sites. For *Homo sapiens*, we further divided the splice sites and the control dinucleotides into two
570 groups, depending on whether they were subject to CpG hypermutability or not.

571 **Impact of the drift-barrier on genome-wide AS rates: sketched model**

572 To illustrate the impact of the drift barrier, we sketched a simple model, with three hypothetical species of
573 different N_e (low, medium and high N_e). In each species, the repertoire of SVs consists of two categories:
574 functional variants and spurious variants (which result from errors of the splicing machinery). The rate of
575 splicing error was assumed to be low and to depend on N_e , owing to the drift barrier effect. We considered
576 that in all species, only a small fraction of **major** introns (5%) produce functional SVs, but that these variants
577 have a relatively high AS rate. The AS rates of functional SVs were modeled by a normal distribution,
578 with a mean of 25% and a standard deviation of 5% (same parameters for the three species). We modeled
579 the distribution of error rates by a gamma distribution, with shape parameter = 1, and with mean values
580 of 0.2%, 0.6% and 1.2% respectively in species of high, medium or low N_e (these parameters were set to
581 match approximately the AS rates observed in empirical data for rare SVs). We then combined the two
582 distributions (functional SVs and splicing errors) to compute the genome-wide average AS rates in each
583 species. We also computed the average AS rate on the subsets of low-AS or high-AS **major** introns (*i.e.* with
584 AS rates respectively below or above the threshold AS rate of 5%). Finally, we computed the proportion
585 of frame-preserving SVs among high-AS **major** introns, assuming that two thirds of splicing errors induce
586 frameshifts and that all functional SVs preserve the reading frame.

587 **Acknowledgements**

588 We thank Loïc Guille for his contribution to an initial pilot study, Tristan Lefébure for insightful discussions
589 and Laurent Guéguen for his help on ***dN/dS*** analyses. Computational analyses were performed using the
590 computing facilities of the CC LBBE/PRABI and the Core Cluster of the Institut Français de Bioinformatique
591 (IFB) (ANR-11-INBS-0013).

592 **Funding**

593 This work was funded by the French National Research Agency (ANR-20-CE02-0008-01 "NeGA" and
594 ANR-17-CE12-0019-01 "LncEvoSys").

595 **Conflict of interest disclosure**

596 The authors declare the following non-financial conflict of interest: Laurent Duret is recommender for PCI
597 Evol Biol.

598 **Data and code availability**

599 All processed data that we generated and used in this study, as well as the scripts that we used to analyze the
600 data and to generate the figures, are available on zenodo DOI: <https://doi.org/10.5281/zenodo.7789408>.
601

602 In particular, the sources of transcriptomic data, genome assemblies and annotations are reported in the
603 Zenodo archive in [data/Data1-suppl.tab](#). The archive includes several directories, including [figure](#), which
604 contains the necessary materials to produce the figures of the manuscript. Rmarkdown scripts located in
605 the [table_suppl](#) directory were used to generate supplementary tables, which are also saved in the same
606 directory. The processed data used to generate figures and conduct analyses are stored in the [data](#) directory
607 in tab-separated text format.

608 **References**

- 609 Abascal, F., Ezkurdia, I., Rodriguez-Rivas, J., Rodriguez, J. M., Pozo, A. d., Vázquez, J., Valencia, A.,
610 and Tress, M. L. 2015. Alternatively Spliced Homologous Exons Have Ancient Origins and Are Highly
611 Expressed at the Protein Level. *PLOS Computational Biology*, 11(6): e1004325. Publisher: Public Library
612 of Science.
- 613 Auton, A., Abecasis, G. R., Altshuler, D. M., Durbin, R. M., Abecasis, G. R., Bentley, D. R., Chakravarti,
614 A., Clark, A. G., Donnelly, P., Eichler, E. E., Flicek, P., Gabriel, S. B., Gibbs, R. A., Green, E. D., Hurles,
615 M. E., Knoppers, B. M., Korbel, J. O., Lander, E. S., Lee, C., Leirach, H., Mardis, E. R., Marth, G. T.,
616 McVean, G. A., Nickerson, D. A., Schmidt, J. P., Sherry, S. T., Wang, J., Wilson, R. K., Gibbs, R. A.,
617 Boerwinkle, E., Doddapaneni, H., Han, Y., Korchina, V., Kovar, C., Lee, S., Muzny, D., Reid, J. G., Zhu,
618 Y., Wang, J., Chang, Y., Feng, Q., Fang, X., Guo, X., Jian, M., Jiang, H., Jin, X., Lan, T., Li, G., Li, J., Li,
619 Y., Liu, S., Liu, X., Lu, Y., Ma, X., Tang, M., Wang, B., Wang, G., Wu, H., Wu, R., Xu, X., Yin, Y., Zhang,
620 D., Zhang, W., Zhao, J., Zhao, M., Zheng, X., Lander, E. S., Altshuler, D. M., Gabriel, S. B., Gupta, N.,
621 Gharani, N., Toji, L. H., Gerry, N. P., Resch, A. M., Flicek, P., Barker, J., Clarke, L., Gil, L., Hunt, S. E.,
622 Kelman, G., Kulesha, E., Leinonen, R., McLaren, W. M., Radhakrishnan, R., Roa, A., Smirnov, D., Smith,
623 R. E., Streeter, I., Thormann, A., Toneva, I., Vaughan, B., Zheng-Bradley, X., Bentley, D. R., Grocock, R.,
624 Humphray, S., James, T., Kingsbury, Z., Leirach, H., Sudbrak, R., Albrecht, M. W., Amstislavskiy, V. S.,
625 Borodina, T. A., Lienhard, M., Mertes, F., Sultan, M., Timmermann, B., Yaspo, M.-L., Mardis, E. R.,

- 626 Wilson, R. K., Fulton, L., Fulton, R., Sherry, S. T., Ananiev, V., Belaia, Z., Beloslyudtsev, D., Bouk, N.,
627 Chen, C., Church, D., Cohen, R., Cook, C., Garner, J., Hefferon, T., Kimelman, M., Liu, C., Lopez, J.,
628 Meric, P., O’Sullivan, C., Ostapchuk, Y., Phan, L., Ponomarov, S., Schneider, V., Shekhtman, E., Sirotkin,
629 K., Slotta, D., Zhang, H., McVean, G. A., Durbin, R. M., Balasubramaniam, S., Burton, J., Danecek, P.,
630 Keane, T. M., Kolb-Kokocinski, A., McCarthy, S., Stalker, J., Quail, M., Schmidt, J. P., Davies, C. J.,
631 Gollub, J., Webster, T., Wong, B., Zhan, Y., Auton, A., Campbell, C. L., Kong, Y., Marcketta, A., Gibbs,
632 R. A., Yu, F., Antunes, L., Bainbridge, M., Muzny, D., Sabo, A., Huang, Z., Wang, J., Coin, L. J. M.,
633 Fang, L., Guo, X., Jin, X., Li, G., Li, Q., Li, Y., Li, Z., Lin, H., Liu, B., Luo, R., Shao, H., Xie, Y.,
634 Ye, C., Yu, C., Zhang, F., Zheng, H., Zhu, H., Alkan, C., Dal, E., Kahveci, F., Marth, G. T., Garrison,
635 E. P., Kural, D., Lee, W.-P., Fung Leong, W., Stromberg, M., Ward, A. N., Wu, J., Zhang, M., Daly,
636 M. J., DePristo, M. A., Handsaker, R. E., Altshuler, D. M., Banks, E., Bhatia, G., del Angel, G., Gabriel,
637 S. B., Genovese, G., Gupta, N., Li, H., Kashin, S., Lander, E. S., McCarroll, S. A., Nemes, J. C., Poplin,
638 R. E., Yoon, S. C., Lihm, J., Makarov, V., Clark, A. G., Gottipati, S., Keinan, A., Rodriguez-Flores,
639 J. L., Korb, J. O., Rausch, T., Fritz, M. H., Stütz, A. M., Flicek, P., Beal, K., Clarke, L., Datta, A.,
640 Herrero, J., McLaren, W. M., Ritchie, G. R. S., Smith, R. E., Zerbino, D., Zheng-Bradley, X., Sabeti,
641 P. C., Shlyakhter, I., Schaffner, S. F., Vitti, J., Cooper, D. N., Ball, E. V., Stenson, P. D., Bentley, D. R.,
642 Barnes, B., Bauer, M., Keira Cheetham, R., Cox, A., Eberle, M., Humphray, S., Kahn, S., Murray, L.,
643 Peden, J., Shaw, R., Kenny, E. E., Batzer, M. A., Konkel, M. K., Walker, J. A., MacArthur, D. G., Lek,
644 M., Sudbrak, R., Amstislavskiy, V. S., Herwig, R., Mardis, E. R., Ding, L., Koboldt, D. C., Larson, D.,
645 Ye, K., Gravel, S., The 1000 Genomes Project Consortium, Corresponding authors, Steering committee,
646 Production group, Baylor College of Medicine, BGI-Shenzhen, Broad Institute of MIT and Harvard, Coriell
647 Institute for Medical Research, European Molecular Biology Laboratory, E. B. I., Illumina, Max Planck
648 Institute for Molecular Genetics, McDonnell Genome Institute at Washington University, US National
649 Institutes of Health, University of Oxford, Wellcome Trust Sanger Institute, Analysis group, Affymetrix,
650 Albert Einstein College of Medicine, Bilkent University, Boston College, Cold Spring Harbor Laboratory,
651 Cornell University, European Molecular Biology Laboratory, Harvard University, Human Gene Mutation
652 Database, Icahn School of Medicine at Mount Sinai, Louisiana State University, Massachusetts General
653 Hospital, McGill University, and National Eye Institute, N. 2015. A global reference for human genetic
654 variation. *Nature*, 526(7571): 68–74. Number: 7571 Publisher: Nature Publishing Group.
- 655 Barbosa-Morais, N. L., Irimia, M., Pan, Q., Xiong, H. Y., Gueroussov, S., Lee, L. J., Slobodeniuc, V., Kutter,
656 C., Watt, S., Colak, R., Kim, T., Misquitta-Ali, C. M., Wilson, M. D., Kim, P. M., Odom, D. T., Frey,
657 B. J., and Blencowe, B. J. 2012. The evolutionary landscape of alternative splicing in vertebrate species.
658 *Science (New York, N.Y.)*, 338(6114): 1587–1593.
- 659 Bhuiyan, S. A., Ly, S., Phan, M., Huntington, B., Hogan, E., Liu, C. C., Liu, J., and Pavlidis, P. 2018.
660 Systematic evaluation of isoform function in literature reports of alternative splicing. *BMC Genomics*,
661 19(1): 637.
- 662 Blencowe, B. J. 2017. The Relationship between Alternative Splicing and Proteomic Complexity. *Trends in*
663 *Biochemical Sciences*, 42(6): 407–408. Publisher: Elsevier.

- 664 Bolívar, P., Guéguen, L., Duret, L., Ellegren, H., and Mugal, C. F. 2019. GC-biased gene conversion conceals
665 the prediction of the nearly neutral theory in avian genomes. *Genome Biology*, 20(1): 5.
- 666 Bush, S. J., Chen, L., Tovar-Corona, J. M., and Urrutia, A. O. 2017. Alternative splicing and the evolution
667 of phenotypic novelty. *Philosophical Transactions of the Royal Society B: Biological Sciences*, 372(1713):
668 20150474. Publisher: Royal Society.
- 669 Cardoso-Moreira, M., Halbert, J., Valloton, D., Velten, B., Chen, C., Shao, Y., Liechti, A., Ascenção, K.,
670 Rummel, C., Ovchinnikova, S., Mazin, P. V., Xenarios, I., Harshman, K., Mort, M., Cooper, D. N.,
671 Sandi, C., Soares, M. J., Ferreira, P. G., Afonso, S., Carneiro, M., Turner, J. M. A., VandeBerg, J. L.,
672 Fallahshahroudi, A., Jensen, P., Behr, R., Lisgo, S., Lindsay, S., Khaitovich, P., Huber, W., Baker, J.,
673 Anders, S., Zhang, Y. E., and Kaessmann, H. 2019. Gene expression across mammalian organ development.
674 *Nature*, 571(7766): 505–509.
- 675 Charif, D. and Lobry, J. R. 2007. SeqinR 1.0-2: A Contributed Package to the R Project for Statistical
676 Computing Devoted to Biological Sequences Retrieval and Analysis. In U. Bastolla, M. Porto, H. E.
677 Roman, and M. Vendruscolo, editors, *Structural Approaches to Sequence Evolution: Molecules, Networks,*
678 *Populations*, Biological and Medical Physics, Biomedical Engineering, pages 207–232. Springer, Berlin,
679 Heidelberg.
- 680 Chen, L., Bush, S. J., Tovar-Corona, J. M., Castillo-Morales, A., and Urrutia, A. O. 2014. Correcting for
681 Differential Transcript Coverage Reveals a Strong Relationship between Alternative Splicing and Organism
682 Complexity. *Molecular Biology and Evolution*, 31(6): 1402–1413.
- 683 Dutheil, J. and Boussau, B. 2008. Non-homogeneous models of sequence evolution in the Bio++ suite of
684 libraries and programs. *BMC Evolutionary Biology*, 8(1): 255.
- 685 Dutheil, J. Y., Galtier, N., Romiguier, J., Douzery, E. J. P., Ranwez, V., and Boussau, B. 2012. Efficient
686 selection of branch-specific models of sequence evolution. *Molecular Biology and Evolution*, 29(7): 1861–
687 1874.
- 688 Figuet, E., Nabholz, B., Bonneau, M., Mas Carrio, E., Nadachowska-Brzyska, K., Ellegren, H., and Galtier,
689 N. 2016. Life History Traits, Protein Evolution, and the Nearly Neutral Theory in Amniotes. *Molecular*
690 *Biology and Evolution*, 33(6): 1517–1527.
- 691 Freckleton, R., Harvey, P., and Pagel, M. 2002. Phylogenetic Analysis and Comparative Data: A Test and
692 Review of Evidence. *The American naturalist*, 160: 712–26.
- 693 González-Porta, M., Frankish, A., Rung, J., Harrow, J., and Brazma, A. 2013. Transcriptome analysis of
694 human tissues and cell lines reveals one dominant transcript per gene. *Genome Biology*, 14(7): 1–11.
695 Number: 7 Publisher: BioMed Central.
- 696 Gout, J.-F., Thomas, W. K., Smith, Z., Okamoto, K., and Lynch, M. 2013. Large-scale detection of in vivo
697 transcription errors. *Proceedings of the National Academy of Sciences*, 110(46): 18584–18589. Publisher:
698 Proceedings of the National Academy of Sciences.

- 699 Graveley, B. R. 2001. Alternative splicing: increasing diversity in the proteomic world. *Trends in Genetics*,
700 17(2): 100–107.
- 701 Guéguen, L. and Duret, L. 2018. Unbiased Estimate of Synonymous and Nonsynonymous Substitution Rates
702 with Nonstationary Base Composition. *Molecular Biology and Evolution*, 35(3): 734–742.
- 703 Guéguen, L., Gaillard, S., Boussau, B., Gouy, M., Groussin, M., Rochette, N. C., Bigot, T., Fournier, D.,
704 Pouyet, F., Cahais, V., Bernard, A., Scornavacca, C., Nabholz, B., Haudry, A., Dachary, L., Galtier, N.,
705 Belkhir, K., and Dutheil, J. Y. 2013. Bio++: efficient extensible libraries and tools for computational
706 molecular evolution. *Molecular Biology and Evolution*, 30(8): 1745–1750.
- 707 Hamid, F. M. and Makeyev, E. V. 2014. Emerging functions of alternative splicing coupled with nonsense-
708 mediated decay. *Biochemical Society Transactions*, 42(4): 1168–1173.
- 709 Hinrichs, A. S., Karolchik, D., Baertsch, R., Barber, G. P., Bejerano, G., Clawson, H., Diekhans, M., Furey,
710 T. S., Harte, R. A., Hsu, F., Hillman-Jackson, J., Kuhn, R. M., Pedersen, J. S., Pohl, A., Raney, B. J.,
711 Rosenbloom, K. R., Siepel, A., Smith, K. E., Sugnet, C. W., Sultan-Qurraie, A., Thomas, D. J., Trumbower,
712 H., Weber, R. J., Weirauch, M., Zweig, A. S., Haussler, D., and Kent, W. J. 2006. The UCSC Genome
713 Browser Database: update 2006. *Nucleic Acids Research*, 34(Database issue): D590–D598.
- 714 Hsu, S.-N. and Hertel, K. J. 2009. Spliceosomes walk the line: splicing errors and their impact on cellular
715 function. *RNA biology*, 6(5): 526–530.
- 716 Huang, W., Massouras, A., Inoue, Y., Peiffer, J., Ràmia, M., Tarone, A. M., Turlapati, L., Zichner, T., Zhu,
717 D., Lyman, R. F., Magwire, M. M., Blankenburg, K., Carbone, M. A., Chang, K., Ellis, L. L., Fernandez,
718 S., Han, Y., Highnam, G., Hjelman, C. E., Jack, J. R., Javaid, M., Jayaseelan, J., Kalra, D., Lee, S., Lewis,
719 L., Munidasa, M., Ongeri, F., Patel, S., Perales, L., Perez, A., Pu, L., Rollmann, S. M., Ruth, R., Saada, N.,
720 Warner, C., Williams, A., Wu, Y.-Q., Yamamoto, A., Zhang, Y., Zhu, Y., Anholt, R. R. H., Korbel, J. O.,
721 Mittelman, D., Muzny, D. M., Gibbs, R. A., Barbadilla, A., Johnston, J. S., Stone, E. A., Richards, S.,
722 Deplancke, B., and Mackay, T. F. C. 2014. Natural variation in genome architecture among 205 *Drosophila*
723 *melanogaster* Genetic Reference Panel lines. *Genome Research*, 24(7): 1193–1208. Company: Cold Spring
724 Harbor Laboratory Press Distributor: Cold Spring Harbor Laboratory Press Institution: Cold Spring
725 Harbor Laboratory Press Label: Cold Spring Harbor Laboratory Press Publisher: Cold Spring Harbor Lab.
- 726 John, S., Olas, J. J., and Mueller-Roeber, B. 2021. Regulation of alternative splicing in response to temperature
727 variation in plants. *Journal of Experimental Botany*, 72(18): 6150–6163.
- 728 Kim, D., Paggi, J. M., Park, C., Bennett, C., and Salzberg, S. L. 2019. Graph-based genome alignment
729 and genotyping with HISAT2 and HISAT-genotype. *Nature Biotechnology*, 37(8): 907–915. Number: 8
730 Publisher: Nature Publishing Group.
- 731 Kimura, M., Maruyama, T., and Crow, J. F. 1963. The Mutation Load in Small Populations. *Genetics*,
732 48(10): 1303–1312.
- 733 Kozlov, A. M., Darriba, D., Flouri, T., Morel, B., and Stamatakis, A. 2019. RAxML-NG: a fast, scalable and
734 user-friendly tool for maximum likelihood phylogenetic inference. *Bioinformatics*, 35(21): 4453–4455.

- 735 Kryazhimskiy, S. and Plotkin, J. B. 2008. The Population Genetics of dN/dS. *PLoS Genetics*, 4(12).
- 736 Leinonen, R., Sugawara, H., and Shumway, M. 2011. The Sequence Read Archive. *Nucleic Acids Research*,
737 39(Database issue): D19–D21.
- 738 Leung, S. K., Jeffries, A. R., Castanho, I., Jordan, B. T., Moore, K., Davies, J. P., Dempster, E. L., Bray,
739 N. J., O’Neill, P., Tseng, E., Ahmed, Z., Collier, D. A., Jeffery, E. D., Prabhakar, S., Schalkwyk, L., Jops,
740 C., Gandal, M. J., Sheynkman, G. M., Hannon, E., and Mill, J. 2021. Full-length transcript sequencing of
741 human and mouse cerebral cortex identifies widespread isoform diversity and alternative splicing. *Cell*
742 *Reports*, 37(7): 110022.
- 743 Li, W. and Lynch, M. 2020. Universally high transcript error rates in bacteria. *eLife*, 9: e54898. Publisher:
744 eLife Sciences Publications, Ltd.
- 745 Liu, Z. and Zhang, J. 2018a. Human C-to-U Coding RNA Editing Is Largely Nonadaptive. *Molecular Biology*
746 *and Evolution*, 35(4): 963–969.
- 747 Liu, Z. and Zhang, J. 2018b. Most m6A RNA Modifications in Protein-Coding Regions Are Evolutionarily
748 Unconserved and Likely Nonfunctional. *Molecular Biology and Evolution*, 35(3): 666–675.
- 749 Lynch, M. 2006. The Origins of Eukaryotic Gene Structure. *Molecular Biology and Evolution*, 23(2): 450–468.
- 750 Lynch, M. 2007. The frailty of adaptive hypotheses for the origins of organismal complexity. *Proceedings*
751 *of the National Academy of Sciences*, 104(suppl.1): 8597–8604. Publisher: Proceedings of the National
752 Academy of Sciences.
- 753 Lynch, M. and Conery, J. S. 2003. The origins of genome complexity. *Science (New York, N.Y.)*, 302(5649):
754 1401–1404.
- 755 Lynch, M., Ackerman, M. S., Gout, J.-F., Long, H., Sung, W., Thomas, W. K., and Foster, P. L. 2016.
756 Genetic drift, selection and the evolution of the mutation rate. *Nature Reviews Genetics*, 17(11): 704–714.
757 Number: 11 Publisher: Nature Publishing Group.
- 758 Löytynoja, A. and Goldman, N. 2008. Phylogeny-Aware Gap Placement Prevents Errors in Sequence
759 Alignment and Evolutionary Analysis. *Science*, 320(5883): 1632–1635. Publisher: American Association
760 for the Advancement of Science.
- 761 Mackay, T. F. C., Richards, S., Stone, E. A., Barbadilla, A., Ayroles, J. F., Zhu, D., Casillas, S., Han, Y.,
762 Magwire, M. M., Cridland, J. M., Richardson, M. F., Anholt, R. R. H., Barrón, M., Bess, C., Blankenburg,
763 K. P., Carbone, M. A., Castellano, D., Chaboub, L., Duncan, L., Harris, Z., Javaid, M., Jayaseelan, J. C.,
764 Jhangiani, S. N., Jordan, K. W., Lara, F., Lawrence, F., Lee, S. L., Librado, P., Linheiro, R. S., Lyman,
765 R. F., Mackey, A. J., Munidasa, M., Muzny, D. M., Nazareth, L., Newsham, I., Perales, L., Pu, L.-L., Qu,
766 C., Ràmia, M., Reid, J. G., Rollmann, S. M., Rozas, J., Saada, N., Turlapati, L., Worley, K. C., Wu, Y.-Q.,
767 Yamamoto, A., Zhu, Y., Bergman, C. M., Thornton, K. R., Mittelman, D., and Gibbs, R. A. 2012. The
768 *Drosophila melanogaster* Genetic Reference Panel. *Nature*, 482(7384): 173–178. Number: 7384 Publisher:
769 Nature Publishing Group.

- 770 Mazin, P. V., Khaitovich, P., Cardoso-Moreira, M., and Kaessmann, H. 2021. Alternative splicing during
771 mammalian organ development. *Nature Genetics*, 53(6): 925–934. Number: 6 Publisher: Nature Publishing
772 Group.
- 773 McGlincy, N. J. and Smith, C. W. J. 2008. Alternative splicing resulting in nonsense-mediated mRNA decay:
774 what is the meaning of nonsense? *Trends in Biochemical Sciences*, 33(8): 385–393.
- 775 Merkin, J., Russell, C., Chen, P., and Burge, C. B. 2012. Evolutionary dynamics of gene and isoform
776 regulation in Mammalian tissues. *Science (New York, N.Y.)*, 338(6114): 1593–1599.
- 777 Mudge, J. M., Frankish, A., Fernandez-Banet, J., Alioto, T., Derrien, T., Howald, C., Reymond, A., Guigó,
778 R., Hubbard, T., and Harrow, J. 2011. The Origins, Evolution, and Functional Potential of Alternative
779 Splicing in Vertebrates. *Molecular Biology and Evolution*, 28(10): 2949–2959.
- 780 NCBI Resource Coordinators 2018. Database resources of the National Center for Biotechnology Information.
781 *Nucleic Acids Research*, 46(D1): D8–D13.
- 782 Ohta, T. 1973. Slightly Deleterious Mutant Substitutions in Evolution. *Nature*, 246(5428): 96–98. Number:
783 5428 Publisher: Nature Publishing Group.
- 784 Pickrell, J. K., Pai, A. A., Gilad, Y., and Pritchard, J. K. 2010. Noisy Splicing Drives mRNA Isoform
785 Diversity in Human Cells. *PLOS Genetics*, 6(12): e1001236. Publisher: Public Library of Science.
- 786 Rajon, E. and Masel, J. 2011. Evolution of molecular error rates and the consequences for evolvability.
787 *Proceedings of the National Academy of Sciences of the United States of America*, 108(3): 1082–1087.
- 788 Reyes, A., Anders, S., Weatheritt, R. J., Gibson, T. J., Steinmetz, L. M., and Huber, W. 2013. Drift
789 and conservation of differential exon usage across tissues in primate species. *Proceedings of the National
790 Academy of Sciences*, 110(38): 15377–15382. Publisher: Proceedings of the National Academy of Sciences.
- 791 Roberts, A., Pimentel, H., Trapnell, C., and Pachter, L. 2011. Identification of novel transcripts in annotated
792 genomes using RNA-Seq. *Bioinformatics*, 27(17): 2325–2329.
- 793 Saudemont, B., Popa, A., Parmley, J. L., Rocher, V., Blugeon, C., Necsulea, A., Meyer, E., and Duret, L.
794 2017. The fitness cost of mis-splicing is the main determinant of alternative splicing patterns. *Genome
795 Biology*, 18.
- 796 Seppy, M., Manni, M., and Zdobnov, E. M. 2019. BUSCO: Assessing Genome Assembly and Annotation
797 Completeness. *Methods in Molecular Biology (Clifton, N.J.)*, 1962: 227–245.
- 798 Singh, P. and Ahi, E. P. 2022. The importance of alternative splicing in adaptive evolution. *Molecular
799 Ecology*, 31(7): 1928–1938. Publisher: John Wiley & Sons, Ltd.
- 800 Tomso, D. J. and Bell, D. A. 2003. Sequence Context at Human Single Nucleotide Polymorphisms: Over-
801 representation of CpG Dinucleotide at Polymorphic Sites and Suppression of Variation in CpG Islands.
802 *Journal of Molecular Biology*, 327(2): 303–308.

- 803 Traverse, C. C. and Ochman, H. 2016. From the Cover: Conserved rates and patterns of transcription errors
804 across bacterial growth states and lifestyles. *Proceedings of the National Academy of Sciences of the United*
805 *States of America*, 113(12): 3311. Publisher: National Academy of Sciences.
- 806 Tress, M. L., Abascal, F., and Valencia, A. 2017a. Alternative Splicing May Not Be the Key to Proteome
807 Complexity. *Trends in Biochemical Sciences*, 42(2): 98–110.
- 808 Tress, M. L., Abascal, F., and Valencia, A. 2017b. Most Alternative Isoforms Are Not Functionally Important.
809 *Trends in biochemical sciences*, 42(6): 408–410.
- 810 Verta, J.-P. and Jacobs, A. 2022. The role of alternative splicing in adaptation and evolution. *Trends in*
811 *Ecology & Evolution*, 37(4): 299–308.
- 812 Waples, R. S. 2016. Life-history traits and effective population size in species with overlapping generations
813 revisited: the importance of adult mortality. *Heredity*, 117(4): 241–250.
- 814 Weyna, A. and Romiguier, J. 2020. Relaxation of purifying selection suggests low effective population size in
815 eusocial Hymenoptera and solitary pollinating bees. *bioRxiv*, page 2020.04.14.038893. Publisher: Cold
816 Spring Harbor Laboratory Section: New Results.
- 817 Wright, C. J., Smith, C. W. J., and Jiggins, C. D. 2022. Alternative splicing as a source of phenotypic
818 diversity. *Nature Reviews Genetics*, 23(11): 697–710. Number: 11 Publisher: Nature Publishing Group.
- 819 Xiong, K., McEntee, J. P., Porfirio, D. J., and Masel, J. 2017. Drift Barriers to Quality Control When Genes
820 Are Expressed at Different Levels. *Genetics*, 205(1): 397–407.
- 821 Xu, C. and Zhang, J. 2018. Alternative polyadenylation of mammalian transcripts is generally deleterious,
822 not adaptive. *Cell systems*, 6(6): 734–742.e4.
- 823 Xu, C. and Zhang, J. 2020. A different perspective on alternative cleavage and polyadenylation. *Nature*
824 *Reviews Genetics*, 21(1): 63–63. Number: 1 Publisher: Nature Publishing Group.
- 825 Xu, C., Park, J.-K., and Zhang, J. 2019. Evidence that alternative transcriptional initiation is largely
826 nonadaptive. *PLoS Biology*, 17(3): e3000197.
- 827 Xu, G. and Zhang, J. 2014. Human coding RNA editing is generally nonadaptive. *Proceedings of the National*
828 *Academy of Sciences*, 111(10): 3769–3774. Publisher: Proceedings of the National Academy of Sciences.
- 829 Yang, Z. and Nielsen, R. 1998. Synonymous and nonsynonymous rate variation in nuclear genes of mammals.
830 *Journal of Molecular Evolution*, 46(4): 409–418.
- 831 Zhang, J. and Xu, C. 2022. Gene product diversity: adaptive or not? *Trends in Genetics*, 38(11): 1112–1122.

RANDOM GENETIC DRIFT SETS AN UPPER LIMIT ON mRNA SPLICING ACCURACY IN METAZOANS

Supplementary Table 1: Description of the main features of the samples analyzed in this study.

	Clade	Number of RNA-seq samples	Sequencing depth (per-base read) ^a	Number of annotated introns	Number of analyzable introns ^b	Average number of introns per BUSCO gene	Fraction of major introns alternatively spliced ^c	Average AS rate among BUSCO introns	Fraction of rare SVs ^d
Vertebrates									
<i>Callorhynchus milii</i>	Chondrichthyes	11	1068	7700	7467	8.0	0.491	1.47 %	0.831
<i>Gallus gallus</i>	Aves	217	9657	8741	8621	8.4	0.854	1.59 %	0.958
<i>Crocodylus porosus</i>	Crocodylia	12	1819	7867	7668	8.5	0.817	3.02 %	0.908
<i>Monodelphis domestica</i>	Mammalia	269	11371	8538	8407	8.5	0.915	1.91 %	0.957
<i>Heterocephalus glaber</i>	Mammalia	54	2072	9409	9324	8.6	0.803	2.69 %	0.914
<i>Macaca mulatta</i>	Mammalia	177	5571	9328	9261	8.6	0.908	2.84 %	0.948
<i>Oryctolagus cuniculus</i>	Mammalia	338	15503	8036	7885	8.4	0.950	1.97 %	0.969
<i>Rattus norvegicus</i>	Mammalia	362	16611	8469	8196	8.5	0.953	1.89 %	0.965
<i>Mus musculus</i>	Mammalia	317	12245	9327	9080	8.4	0.937	1.87 %	0.958
<i>Bos taurus</i>	Mammalia	26	710	9046	8926	8.5	0.511	1.63 %	0.856
<i>Loxodonta africana</i>	Mammalia	23	3667	9000	8652	8.3	0.896	3.55 %	0.938
<i>Sus scrofa</i>	Mammalia	55	910	8982	8798	8.5	0.644	1.95 %	0.886
<i>Canis lupus</i>	Mammalia	5	348	9279	8628	8.2	0.436	2.18 %	0.764
<i>Homo sapiens</i>	Mammalia	313	10269	11122	10981	8.4	0.957	3.38 %	0.949
<i>Equus caballus</i>	Mammalia	19	998	9190	9072	8.5	0.658	2.16 %	0.884
Insects									
<i>Bombyx mori</i>	Lepidoptera	14	459	5001	4681	5.3	0.393	1.12 %	0.835
<i>Athalia rosae</i>	Hymenoptera	6	350	4772	4701	4.8	0.348	1.6 %	0.782
<i>Cephus cinctus</i>	Hymenoptera	17	2566	5035	5016	4.7	0.744	2.4 %	0.907
<i>Orussus abietinus</i>	Hymenoptera	2	197	4801	4664	4.7	0.370	2.03 %	0.763
<i>Nasonia vitripennis</i>	Hymenoptera	114	4871	4273	4158	4.5	0.648	1.21 %	0.913
<i>Trichogramma pretiosum</i>	Hymenoptera	4	350	3794	3734	4.4	0.268	0.98 %	0.782
<i>Harpegnathos saltator</i>	Hymenoptera	166	1888	4745	4711	4.7	0.565	2.02 %	0.886
<i>Linepithema humile</i>	Hymenoptera	23	1476	4726	4615	4.8	0.570	1.45 %	0.882
<i>Camponotus floridanus</i>	Hymenoptera	37	449	4596	4546	4.7	0.358	1.52 %	0.761
<i>Pogonomyrmex barbatus</i>	Hymenoptera	39	1388	4678	4440	4.5	0.579	1.91 %	0.866
<i>Polistes canadensis</i>	Hymenoptera	14	440	4665	4562	4.8	0.424	1.88 %	0.834
<i>Polistes dominula</i>	Hymenoptera	12	218	4698	4161	4.3	0.180	1.63 %	0.624
<i>Solenopsis invicta</i>	Hymenoptera	23	436	4516	4394	4.6	0.430	1.71 %	0.807
<i>Acromyrmex echinatior</i>	Hymenoptera	42	1470	4716	4638	4.7	0.529	2.15 %	0.835
<i>Megachile rotundata</i>	Hymenoptera	108	3400	5120	5086	4.8	0.898	3.81 %	0.927
<i>Apis mellifera</i>	Hymenoptera	40	1777	4939	4897	4.9	0.673	2.3 %	0.892
<i>Apis florea</i>	Hymenoptera	4	503	4881	4332	4.4	0.318	1.85 %	0.711
<i>Apis cerana</i>	Hymenoptera	12	1401	4508	4439	4.6	0.578	2.36 %	0.839
<i>Bombus terrestris</i>	Hymenoptera	33	2648	4857	4683	4.7	0.763	2.33 %	0.922
<i>Acyrtosiphon pisum</i>	Hemiptera	35	3163	4918	4844	6.0	0.709	1.09 %	0.933
<i>Cimex lectularius</i>	Hemiptera	10	462	5640	5588	6.3	0.431	1.61 %	0.838
<i>Halyomorpha halys</i>	Hemiptera	6	1460	5715	5676	6.5	0.591	1.73 %	0.885
<i>Aedes aegypti</i>	Diptera	27	2469	2369	2290	2.6	0.514	1.35 %	0.870
<i>Drosophila grimshawi</i>	Diptera	30	256	2190	2032	2.7	0.168	0.8 %	0.726
<i>Drosophila pseudoobscura</i>	Diptera	32	3628	2312	2244	2.6	0.433	1.32 %	0.871
<i>Drosophila melanogaster</i>	Diptera	129	4542	2414	2390	2.7	0.551	1.22 %	0.909
<i>Drosophila suzukii</i>	Diptera	23	1979	2187	2052	2.6	0.287	1.17 %	0.810
<i>Ceratitis capitata</i>	Diptera	29	1168	3067	3015	3.3	0.418	1.45 %	0.860
<i>Lucilia cuprina</i>	Diptera	23	2446	2566	2405	2.8	0.268	0.85 %	0.823
<i>Musca domestica</i>	Diptera	12	1056	2545	2401	2.9	0.254	0.98 %	0.795
<i>Orthophagus taurus</i>	Coleoptera	53	644	2836	2753	3.2	0.377	1.34 %	0.810
<i>Tribolium castaneum</i>	Coleoptera	14	2618	3333	3225	3.6	0.556	1.15 %	0.881
<i>Dendroctonus ponderosae</i>	Coleoptera	30	2262	4370	4269	4.9	0.505	1.26 %	0.882
<i>Anoplophora glabripennis</i>	Coleoptera	20	325	3764	3567	4.1	0.299	1.13 %	0.781
<i>Leptinotarsa decemlineata</i>	Coleoptera	21	2071	3372	3132	3.8	0.512	1.21 %	0.883
<i>Blattella germanica</i>	Blattodea	30	943	4911	4454	5.4	0.423	1.26 %	0.827
<i>Cryptotermes secundus</i>	Blattodea	11	481	6471	6391	6.4	0.573	2.32 %	0.832
<i>Zootermopsis nevadensis</i>	Blattodea	53	3944	6727	6613	6.4	0.802	2.36 %	0.927

^a Median per-base read coverage computed on BUSCO gene exons

^b Number of analyzable introns (i.e. with $N_5 + N_4 \geq 10$) among BUSCO genes

^c Proportion of major introns for which alternative splicing has been detected (i.e. with $N_5 > 0$) among BUSCO genes

^d Fraction of rare spliced variants introns (i.e. with MIRA $\leq 5\%$) among all protein-coding genes

Table S1

Supplementary Table 2: Longevity and body length across the 53 metazoans studied.

	Clade	Longevity (Days)	Body length (cm)
Vertebrates			
<i>Callorhinchus milii</i>	Chondrichthyes	2190	120.00
<i>Gallus gallus</i>	Aves	10950	70.00
<i>Crocodylus porosus</i>	Crocodylia	20805	600.00
<i>Homo sapiens</i>	Mammalia	36500	175.00
<i>Loxodonta africana</i>	Mammalia	23725	400.00
<i>Equus caballus</i>	Mammalia	20805	280.00
<i>Macaca mulatta</i>	Mammalia	14600	64.00
<i>Heterocephalus glaber</i>	Mammalia	10950	16.50
<i>Sus scrofa</i>	Mammalia	9855	240.00
<i>Canis lupus</i>	Mammalia	7519	117.00
<i>Bos taurus</i>	Mammalia	7300	245.00
<i>Oryctolagus cuniculus</i>	Mammalia	3285	50.00
<i>Monodelphis domestica</i>	Mammalia	1862	20.00
<i>Mus musculus</i>	Mammalia	1460	9.50
<i>Rattus norvegicus</i>	Mammalia	1387	40.00
Insects			
<i>Bombyx mori</i>	Lepidoptera	50	1.90
<i>Pogonomyrmex barbatus</i>	Hymenoptera	10220	1.10
<i>Acromyrmex echinatior</i>	Hymenoptera	5475	1.40
<i>Camponotus floridanus</i>	Hymenoptera	3650	1.90
<i>Solenopsis invicta</i>	Hymenoptera	2482	0.70
<i>Apis mellifera</i>	Hymenoptera	1095	2.00
<i>Apis florea</i>	Hymenoptera	1095	2.00
<i>Apis cerana</i>	Hymenoptera	1095	2.00
<i>Harpegnathos saltator</i>	Hymenoptera	653	1.70
<i>Polistes canadensis</i>	Hymenoptera	506	2.00
<i>Polistes dominula</i>	Hymenoptera	506	2.00
<i>Linepithema humile</i>	Hymenoptera	365	0.50
<i>Bombus terrestris</i>	Hymenoptera	150	2.50
<i>Megachile rotundata</i>	Hymenoptera	56	1.90
<i>Nasonia vitripennis</i>	Hymenoptera	25	0.30
<i>Athalia rosae</i>	Hymenoptera	12	0.73
<i>Trichogramma pretiosum</i>	Hymenoptera	10	0.04
<i>Cephus cinctus</i>	Hymenoptera	7	0.86
<i>Orussus abietinus</i>	Hymenoptera	7	1.00
<i>Cimex lectularius</i>	Hemiptera	572	0.50
<i>Halyomorpha halys</i>	Hemiptera	112	1.44
<i>Acyrtosiphon pisum</i>	Hemiptera	30	0.25
<i>Drosophila pseudoobscura</i>	Diptera	90	0.20
<i>Musca domestica</i>	Diptera	60	0.70
<i>Drosophila grimshawi</i>	Diptera	50	0.50
<i>Ceratitis capitata</i>	Diptera	50	0.50
<i>Drosophila suzukii</i>	Diptera	38	0.33
<i>Drosophila melanogaster</i>	Diptera	36	0.30
<i>Lucilia cuprina</i>	Diptera	21	0.80
<i>Aedes aegypti</i>	Diptera	14	0.38
<i>Leptinotarsa decemlineata</i>	Coleoptera	365	1.00
<i>Tribolium castaneum</i>	Coleoptera	170	0.50
<i>Onthophagus taurus</i>	Coleoptera	160	1.00
<i>Anoplophora glabripennis</i>	Coleoptera	66	3.50
<i>Dendroctonus ponderosae</i>	Coleoptera	30	0.75
<i>Cryptotermes secundus</i>	Blattodea	4745	0.60
<i>Zootermopsis nevadensis</i>	Blattodea	2300	1.00
<i>Blattella germanica</i>	Blattodea	200	1.59

* The sources from which the lifespan and the body length information was taken are listed in Data9supp.pdf in the Zenodo data repository (see Data and code availability).

Table S2